AMERICAN SOCIETY FOR MICROBIOLOGY | Journal of Virology®

VIRUS-CELL INTERACTIONS

Cell Type-Dependent Escape of Capsid Inhibitors by Simian Immunodeficiency Virus SIVcpz

Augustin Penda Twizerimana,[a] Rachel Scheck,[a] Daniel Becker,[b] Zeli Zhang,[a]* Marianne Wammers,[a] Leandro Avelar,[b] Marc Pflieger,[b] Dieter Häussinger,[a] Thomas Kurz,[b] Holger Gohlke,[b,c,d,e] Carsten Münk[a]

[a]Clinic for Gastroenterology, Hepatology, and Infectiology, Medical Faculty, Heinrich Heine University Düsseldorf, Düsseldorf, Germany
[b]Institute for Pharmaceutical and Medicinal Chemistry, Heinrich Heine University Düsseldorf, Düsseldorf, Germany
[c]John von Neumann Institute for Computing, Forschungszentrum Jülich GmbH, Jülich, Germany
[d]Jülich Supercomputing Centre, Forschungszentrum Jülich GmbH, Jülich, Germany
[e]Institute of Biological Information Processing (IBI-7: Structural Biochemistry), Forschungszentrum Jülich GmbH, Jülich, Germany

Augustin Penda Twizerimana and Rachel Scheck made equal contribution to the execution and analysis of experiments. Author order was determined by additional contribution to drafting of the manuscript by A.P.T.

ABSTRACT Pandemic human immunodeficiency virus type 1 (HIV-1) is the result of the zoonotic transmission of simian immunodeficiency virus (SIV) from the chimpanzee subspecies *Pan troglodytes troglodytes* (SIVcpzPtt). The related subspecies *Pan troglodytes schweinfurthii* is the host of a similar virus, SIVcpzPts, which did not spread to humans. We tested these viruses with small-molecule capsid inhibitors (PF57, PF74, and GS-CA1) that interact with a binding groove in the capsid that is also used by CPSF6. While HIV-1 was sensitive to capsid inhibitors in cell lines, human macrophages, and peripheral blood mononuclear cells (PBMCs), SIVcpzPtt was resistant in rhesus FRhL-2 cells and human PBMCs but was sensitive to PF74 in human HOS and HeLa cells. SIVcpzPts was insensitive to PF74 in FRhL-2 cells, HeLa cells, PBMCs, and macrophages but was inhibited by PF74 in HOS cells. A truncated version of CPSF6 (CPSF6-358) inhibited SIVcpzPtt and HIV-1, while in contrast, SIVcpzPts was resistant to CPSF6-358. Homology modeling of HIV-1, SIVcpzPtt, and SIVcpzPts capsids and binding energy estimates suggest that these three viruses bind similarly to the host proteins cyclophilin A (CYPA) and CPSF6 as well as the capsid inhibitor PF74. Cyclosporine treatment, mutation of the CYPA-binding loop in the capsid, or CYPA knockout eliminated the resistance of SIVcpzPts to PF74 in HeLa cells. These experiments revealed that the antiviral capacity of PF74 is controlled by CYPA in a virus- and cell type-specific manner. Our data indicate that SIVcpz viruses can use infection pathways that escape the antiviral activity of PF74. We further suggest that the antiviral activity of PF74 capsid inhibitors depends on cellular cofactors.

IMPORTANCE HIV-1 originated from SIVcpzPtt but not from the related virus SIVcpzPts, and thus, it is important to describe molecular infection by SIVcpzPts in human cells to understand the zoonosis of SIVs. Pharmacological HIV-1 capsid inhibitors (e.g., PF74) bind a capsid groove that is also a binding site for the cellular protein CPSF6. SIVcpzPts was resistant to PF74 in HeLa cells but sensitive in HOS cells, thus indicating cell line-specific resistance. Both SIVcpz viruses showed resistance to PF74 in human PBMCs. Modulating the presence of cyclophilin A or its binding to capsid in HeLa cells overcame SIVcpzPts resistance to PF74. These results indicate that early cytoplasmic infection events of SIVcpzPts may differ between cell types and affect, in an unknown manner, the antiviral activity of capsid inhibitors. Thus, capsid inhibitors depend on the activity or interaction of currently uncharacterized cellular factors.

Citation Twizerimana AP, Scheck R, Becker D, Zhang Z, Wammers M, Avelar L, Pflieger M, Häussinger D, Kurz T, Gohlke H, Münk C. 2020. Cell type-dependent escape of capsid inhibitors by simian immunodeficiency virus SIVcpz. J Virol 94:e01338-20. https://doi.org/10.1128/JVI.01338-20.

Editor Frank Kirchhoff, Ulm University Medical Center

Address correspondence to Carsten Münk, carsten.muenk@med.uni-duesseldorf.de.

* Present address: Zeli Zhang, La Jolla Institute for Immunology, La Jolla, California, USA.

Received 7 July 2020
Accepted 24 August 2020
Accepted manuscript posted online 9 September 2020
Published 9 November 2020

KEYWORDS HIV-1, PF74, SIVcpz, CPSF6, cyclophilin, zoonosis

After receptor interaction, human immunodeficiency virus type 1 (HIV-1) infects cells by membrane fusion followed by reverse transcription of its viral genomic RNA into double-stranded DNA, which integrates into the host's chromosomal DNA in the nucleus. The capsid (CA) protein builds a cone-shaped core that delivers viral RNAs and enzymes into the cell. This core undergoes structural changes in a poorly described process called uncoating that takes place either in the cytoplasm, at the nuclear pore, or in the nucleus (1–7), where the CA protein interacts with diverse cellular proteins. To inhibit early capsid-dependent steps in viral infection, small compounds that target the CA protein have been developed (8, 9). Prominent examples of cellular human capsid interactors include cyclophilin A (CYPA) (PPIA [peptidylprolyl isomerase A]), TRIM5α (splice variant α tripartite motif-containing protein 5), MX2 (MX dynamin-like GTPase 2), karyopherin TNPO3 (transportin 3), CPSF6 (cleavage and polyadenylation specificity factor 6), and the nuclear pore proteins NUP358 (nucleoporin 358) (also called RANBP2 [RAN binding protein 2]) and NUP153 (nucleoporin 153) (10–17). NUP153, NUP358, CPSF6, and TNPO3 promote HIV-1 nuclear entry and positively influence integration (1, 17–19). Distantly related simian immunodeficiency viruses (SIVs) from African green monkeys (SIVagm) or rhesus macaques (SIVmac) also bind to NUP153 (19). Thus, it is likely that all primate lentiviruses use similar nuclear entry pathways, but NUP153 may not be required for all SIVs (20). HIV-1 is sensitive to human TRIM5α and MX2 as well as to an experimentally expressed truncated version of CPSF6 (CPSF6-358) (13, 14, 17, 21–23). TNPO3 protects HIV-1 from CPSF6-mediated capsid stabilization in the host cell cytoplasm and prevents CPSF6 from accumulating in the cytoplasm. The mislocalization of CPSF6 to the cytoplasm, as in the case of truncated CPSF6-358, results in the inhibition of HIV-1 (24). Oligomeric CPSF6-358 binds and disrupts the core of HIV-1 (25). Mutations in the CA protein can generate HIV-1 variants that are resistant to these restriction factors (17, 23, 24, 26–28).

One of the best-characterized CA inhibitors is PF74 (also called PF-3450074), which binds to CA at the N-terminal domain–C-terminal domain interface between two monomers of the CA hexamer in a pocket that overlaps the CPSF6 interface and is close to the NUP153 binding site (8, 19, 29–31). Treatment of cells with PF74 blocks HIV-1 via cooperative mechanisms of binding to the capsid and perturbs uncoating and reverse transcription at higher concentrations (5 to 10 μM); lower concentrations (up to 2 μM) block HIV-1 after reverse transcription and before nuclear entry but also inhibit in the nucleus (8, 29, 32–35). Capsid inhibitors with a similar binding location are in development for clinical use (36–38).

Pandemic HIV-1 is the result of the zoonotic transmission of simian immunodeficiency virus from the chimpanzee subspecies *Pan troglodytes troglodytes* (SIVcpzPtt). The related chimpanzee subspecies *Pan troglodytes schweinfurthii* is the host of a similar virus, SIVcpzPts, which did not successfully spread to humans (39–41). Like HIV-1, SIVcpzPtt is sensitive to human TRIM5α and MX2 but evolved in humans to counteract restriction by human BST2 (tetherin) and APOBEC3H (39, 42–45). In this study, we compared the sensitivities of HIV-1 and SIVcpz viruses to early cytoplasmic interactors such as CYPA, CPSF6-358, and capsid inhibitors.

RESULTS

Human cell lines are differentially permissive to SIVcpz viruses. We hypothesized that human-adapted HIV-1 and chimpanzee-adapted SIVcpz viruses differ in their capacities to interact with cytoplasmic cellular factors. We decided to study the capsid-interacting proteins CYPA and CPSF6-358 and capsid inhibitors binding in the CPSF6 groove of capsid. To identify suitable cell systems for our experiments, we tested commonly used cell lines with SIVcpzPtt, SIVcpzPts, and HIV-1 vesicular stomatitis virus G (VSV-G)-pseudotyped luciferase reporter viruses. We infected two human cell lines (HeLa and HOS), three simian cell lines (CV-1 from African green monkeys, FRhL-2 from

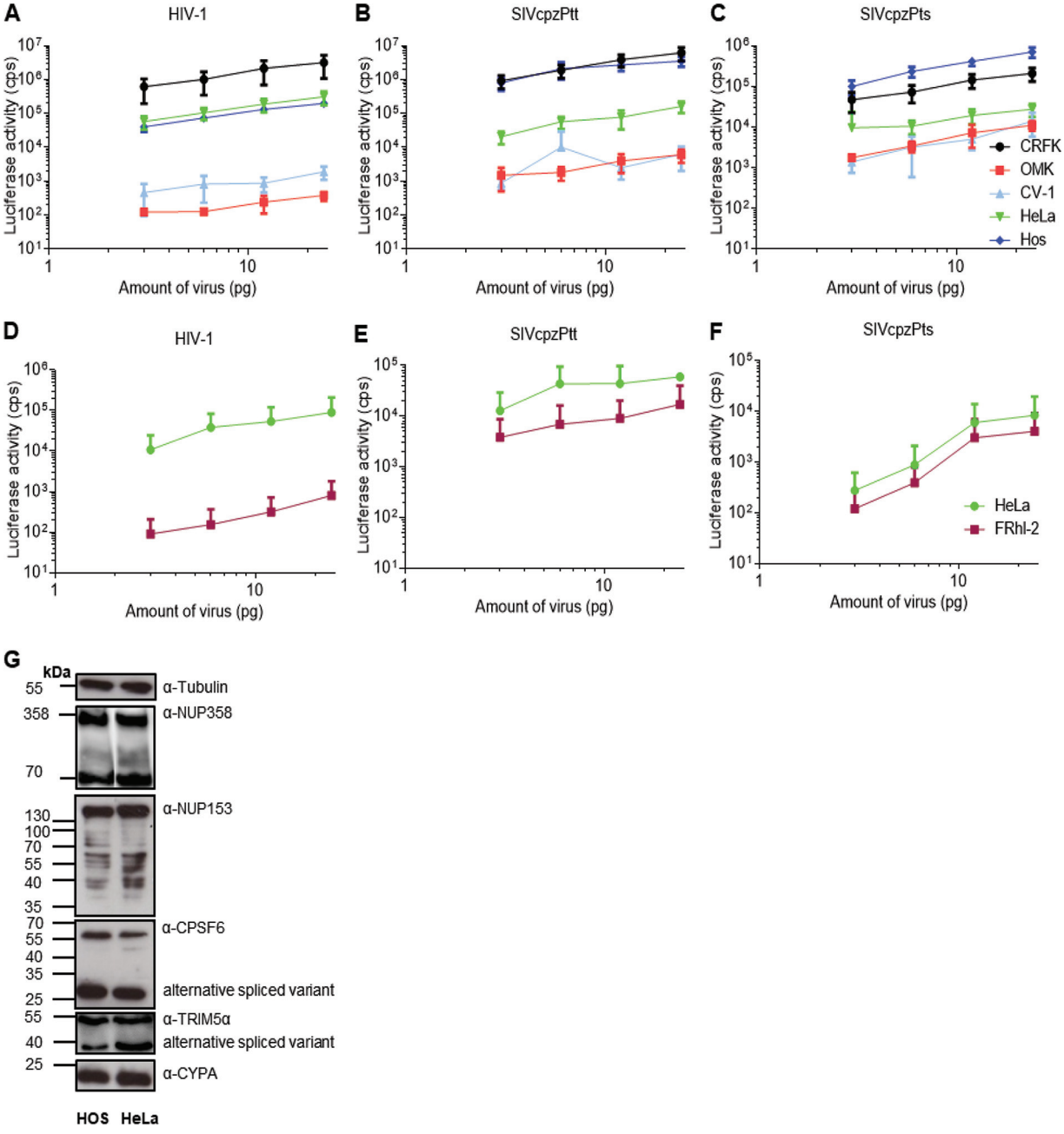

FIG 1 Infection of human and nonhuman cells by HIV-1, SIVcpzPtt, or SIVcpzPts. (A and D) HIV-1 reporter viruses were used to infect CRFK, FRhL-2, OMK, CV-1, HeLa, and HOS cells using increasing amounts of the virus-containing cell supernatant. Firefly luciferase was measured 2 days later. (B, C, E, and F) SIVcpzPtt (B and E) and SIVcpzPts (C and F) reporter viruses were used to infect CRFK, FRhL-2, OMK, CV-1, HeLa, and HOS cells with increasing amounts of the virus-containing cell supernatant. At 2 days postinfection, the activity of nanoluciferase was measured. Values are means with standard deviations (SD). Each experiment was performed at least three times and in triplicates. (G) Expression of HIV-1 host factors in HOS and HeLa cells. Shown are immunoblots of cell lysates of HOS and HeLa cells. Tubulin, NUP358, NUP153, CPSF6, TRIM5α, and CYPA were detected with their specific antibodies. α, anti.

rhesus macaques, and OMK from owl monkeys), and one feline cell line (CRFK) and measured luciferase activity at 2 days postinfection. Feline cells do not express a restricting TRIM5α protein (46), while CV-1 and FRhL-2 cells express TRIM5α proteins and OMK cells express TRIM5Cyp, which inhibit HIV-1 (47). Titration-infection experiments confirmed that both human cell lines were equally permissive to HIV-1, while CRFK cells were 10-fold more susceptible than HeLa or HOS cells, and that HIV-1 was restricted in simian cells (48–50) (Fig. 1A). The difference in infectivity between per-

missive CRFK and restrictive OMK cells was up to 10,000-fold. HIV-1 was slightly more restricted in OMK than in CV-1 cells, but both SIVcpzPtt and SIVcpzPts were equally inhibited in these simian cells (Fig. 1B and C). In further contrast to HIV-1, human HOS cells were more permissive than or equally as permissive as CRFK cells to SIVcpzPtt and SIVcpzPts. For HIV-1 infections, HOS and HeLa cells displayed comparable permissiveness; however, HeLa cells were 33- and 20-fold less infectible by SIVcpzPtt and SIVcpzPts, respectively, than HOS cells. Infection by HIV-1, SIVcpzPtt, and SIVcpzPts was lower in FRhL-2 cells than in HeLa cells, and the differences were the greatest with HIV-1 (Fig. 1D to F). We analyzed the presence of important host proteins in HOS and HeLa cells by immunoblotting and found that the two cell lines express similar amounts of TRIM5α, CYPA, CPSF6, NUP153, and NUP358 (Fig. 1G). Thus, the expression levels of these proteins cannot explain the different sensitivities of HOS and HeLa cells to the two SIVcpz viruses.

SIVcpz viruses show cell type-specific sensitivity to cyclosporine. Cyclophilin A is a cellular protein that has several postulated functions in HIV-1 infection (18, 32, 51–61). CYPA interacts with the capsid of HIV-1 (62) and is incorporated into nascent viral particles (10, 11). In the HIV-1 capsid, CYPA targets a proline-rich loop (also called the CYPA binding loop) with the key interacting residues G89 and P90 (63). Cyclosporine (CsA) is a natural product from a fungus that binds to CYPA and other cyclophilins, and CsA treatment of cells disrupts CYPA incorporation into budding HIV-1 virions (62, 64). HIV-1 mutation of the CYPA binding loop, depletion of CYPA in cells, or inhibition by the use of CsA was instrumental in identifying cell types in which HIV-1 depends on CYPA, such as HOS and primary $CD4^+$ T cells, and cell types in which HIV-1 replicates independently of CYPA, such as HeLa cells (56, 61, 65–71). We aligned the capsid residues of HIV-1 and SIVcpz viruses that are involved in the interaction with CYPA, CPSF6, and capsid inhibitors (Fig. 2A and B; see also Fig. S1 and S2 in the supplemental material). Despite similarities in capsid G89 and P90, which are residues known to be important for the interaction between HIV-1 capsid and CYPA, the alignment highlights differences in the CYPA binding loop on the capsids of HIV-1 and SIVcpz viruses (Fig. 2A and B). Most residues are highly or absolutely conserved within HIV-1 or SIVcpz sequences, respectively, which predominantly also applies to residues interacting with a ligand (marked by stars in Fig. 2A and B). Only residues 91 to 93 that interact with CYPA (blue stars in Fig. 2A and B) show higher sequence variability, also containing nonconservative substitutions within one lineage as well as between lineages. Binding mode models of human CYPA binding to HIV-1, SIVcpzPts, and SIVcpzPtt CA proteins confirmed that the interacting residues differ in 3 positions between HIV-1 CA and SIVcpzPts CA: ILE91 versus GLN91, ALA92 versus GLN92, and PRO93 versus ALA93. The interacting residues differ in 1 position between HIV-1 CA and SIVcpzPtt CA (ALA92 versus PRO92) (Fig. 3A and B).

To identify whether viral particles of SIVcpz and HIV-1 package CYPA in similar manners, immunoblots of virions were analyzed. In virions of SIVcpzPtt and SIVcpzPts, the levels of CYPA were similar to those in HIV-1 particles, and treatment of virus-producing cells with CsA blocked CYPA packaging by all three viruses (Fig. 4A). Glutathione *S*-transferase (GST) pulldown experiments were performed to test the binding of CYPA to SIVcpz GAG. HEK293T cells were cotransfected with plasmids for SIVcpz or HIV-1 and CYPA-GST in the presence or absence of CsA. Following transfection, cells and viruses were lysed, and the lysates were used for pulldown experiments using GST-Sepharose beads. Immunoblotting of the precipitated complexes demonstrated that CYPA-GST interacted with GAG proteins of HIV-1, SIVcpzPtt, and SIVcpzPts (Fig. 4B). Importantly, GST alone did not precipitate GAG, and the administration of 10 μM CsA prevented the binding of CYPA to GAG equally for all three viruses; in contrast, viruses carrying the G89V mutation in the presumed CYPA binding loop of the capsid (Fig. 2A) did not bind CYPA (Fig. 4C).

Since the activity of CYPA in HIV-1 target cells, and not virus-producing cells, regulates HIV-1 replication (56, 68), we treated human HOS and HeLa and rhesus

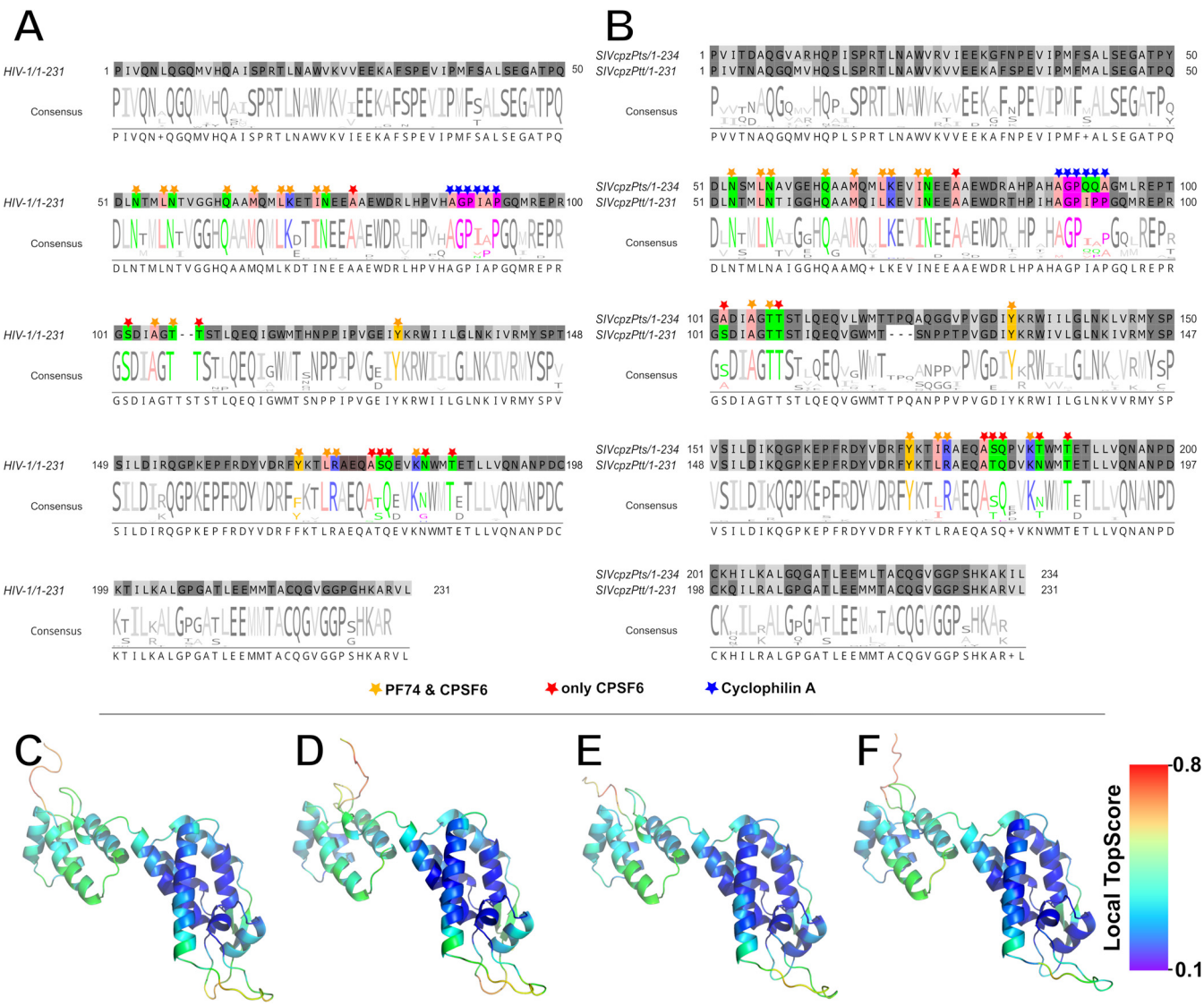

FIG 2 Alignment of CA protein sequences of HIV-1, SIVcpzPts, and SIVcpzPtt and residues engaged in interactions with PF74, CYPA, or CPSF6. (A) HIV-1 CA sequence with the position weight matrix represented as a Weblogo. The HIV-1 CA sequence was taken from the pMDLg/pRRE plasmid. The Weblogo was generated from randomly selected HIV-1 M sequences of different subgroups using MAFFT (108) and Jalview (109) (see also Fig. S1 in the supplemental material). Residues interacting with a ligand are marked with a star. (B) SIVcpz CA sequences (GenBank accession numbers JN835461 and AF447763) with the position weight matrix represented as a Weblogo. The randomly picked SIVcpz CA sequences were retrieved from the Los Alamos HIV and SIV sequence database. The Weblogo was generated from HIV sequences using MAFFT (108) and Jalview (109) (see also Fig. S2 in the supplemental material). Residues interacting with a ligand are marked with a star. For HIV-1 versus SIVcpzPts, the identity was 78.63% and the similarity was 87.18%. For HIV-1 versus SIVcpzPtt, the identity was 89.61% and the similarity was 94.81%. For SIVcpzPts versus SIVcpzPtt, the identity was 78.63% and the similarity was 87.18%. (C to F) Quality assessment of homology models on a per-residue level by TopScore (73). Blue, TopScore of 0.1 (high structural quality); red, TopScore of 0.8 (low structural quality). (C) Homology model of the SIVcpzPts CA monomer based on the structures of HIV-1 CA crystallized with CPSF6 used as the templates. (D) Homology model of the SIVcpzPts CA monomer based on the structures of HIV-1 CA crystallized with PF74 used as the templates. (E) Homology model of the SIVcpzPtt CA monomer based on the structures of HIV-1 CA crystallized with CPSF6 used as the templates. (F) Homology model of the SIVcpzPtt CA monomer based on the structures of HIV-1 CA crystallized with PF74 used as the templates.

macaque FRhL-2 cells with increasing amounts of CsA before infection. Cyclosporine treatment made HOS cells up to 6-fold more resistant to HIV-1 but increased the infection in HeLa and FRhL-2 cells (Fig. 5A). Infections with both SIVcpz viruses demonstrated that CsA treatment of either cell line had no inhibitory consequences and, in fact, stimulated infection (Fig. 5B and C). However, in HOS cells, CsA did not enhance SIVcpzPtt infection (Fig. 5B). To determine whether these observations were related to the CYPA protein, we tried to generate HOS and HeLa *CYPA* knockout (KO) cells (Fig. 6A and B). In HOS cells, the population of cells showed only a weak loss of CYPA protein in immunoblots, and thus, we established and used clonal cell lines that

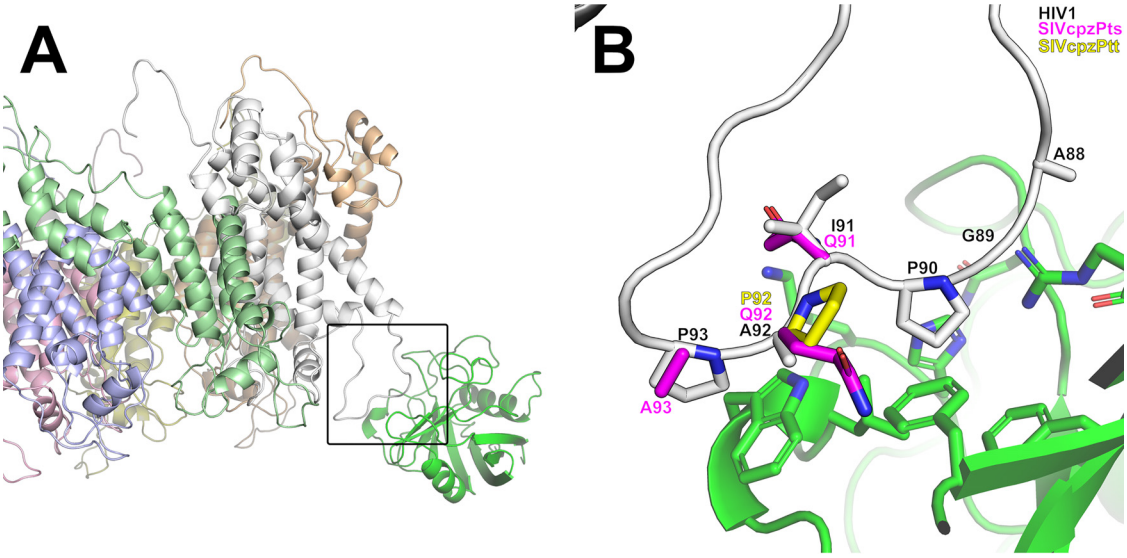

FIG 3 Structural models of binding of human CYPA to HIV-1, SIVcpzPts, and SIVcpzPtt CA proteins. For SIVcpzPts and SIVcpzPtt, CYPA coordinates were taken after superimposing the proteins onto HIV-1 CA bound to CYPA (PDB accession number 5FJB). Monomers are colored differently; the region in the black box in panel A is shown as a blowup in panel B, and side chains of interacting residues are shown as sticks. The interacting residues differ in 3 positions between HIV-1 CA and SIVcpzPts CA: ILE91 versus GLN91, ALA92 versus GLN92, and PRO93 versus ALA93. The interacting residues differ in 1 position between HIV-1 CA and SIVcpzPtt CA (ALA92 versus PRO92).

had a large deficiency in CYPA (Fig. 6A). HOS.CYPA KO clones 1, 3, and 5 showed reduced susceptibility to HIV-1 and SIVcpzPtt but not to SIVcpzPts (Fig. 6C to E). Treatment of HOS.CYPA KO cells with 5 μM CsA during infection did not significantly further increase the restriction of HIV-1 but, surprisingly, reverted the inhibition of SIVcpzPtt (Fig. 6D) and enhanced infections by SIVcpzPts in wild-type (WT) HOS cells and HOS.CYPA KO cells (Fig. 6E). In HeLa cells, we found a significant knockdown (KD) of CYPA in this population of cells, and these HeLa.CYPA KD cells were used for infections (Fig. 6B). CYPA-deficient HeLa cells showed a mild increase in permissiveness to HIV-1 (less than 2-fold) (Fig. 6F) and were 5- to 6-fold more permissive to SIVcpzPtt and SIVcpzPts (Fig. 6G and H). To test the effect of CsA on infection by these viruses in CYPA-deficient HeLa cells, cells were pretreated with 5 μM CsA and infected. Experiments in WT HeLa cells in the presence of CsA revealed data similar to those shown in Fig. 5, and infections by SIVcpzPtt and SIVcpzPts were more enhanced than infection by HIV-1 (Fig. 6F to H). Interestingly, HIV-1 infection was not increased by CsA treatment in HeLa.CYPA KD cells, and its infectivity was reduced by 30% (Fig. 6F). On the other hand, in HeLa.CYPA KD cells, SIVcpzPtt and SIVcpzPts infected 5- and 2-fold more in the presence of CsA, respectively (Fig. 6G and H). Remarkably, the combination of CYPA deficiency and CsA treatment enhanced the permissiveness of HeLa cells to SIVcpzPtt and SIVcpzPts by 30- and 11-fold, respectively. Taken together, these data indicate that CYPA is involved in SIVcpzPtt and SIVcpzPts infection, and for SIVcpzPts, blocking or removing CYPA enhances infection in human HOS and HeLa cells, while SIVcpzPtt enhancement is seen only in HeLa cells. Our data also suggest that CsA treatment influences CYPA-independent pathways of SIVcpz infection.

SIVcpzPts is insensitive to CPSF6-358. To test the effect of CPSF6-358, we generated HOS cells that expressed CPSF6-358 (HOS.CPSF6-358) (Fig. 7A). In HOS.CPSF6-358 cells, infection by HIV-1 was reduced compared to that in HOS cells with the empty vector, while HIV-1 with CA mutants in the CPSF6 binding site (N74D or A77V) (Fig. 2A) (72) escaped this restriction (Fig. 7B to D). CPSF6-358 also inhibited HIV-1 in HOS.CYPA KO cells (Fig. 7B). SIVcpzPtt showed a pattern of restriction in these cell lines similar to that of WT HIV-1 (Fig. 7E). In contrast, CPSF6-358 did not inhibit SIVcpzPts in WT HOS or HOS.CYPA KO cells (Fig. 7F).

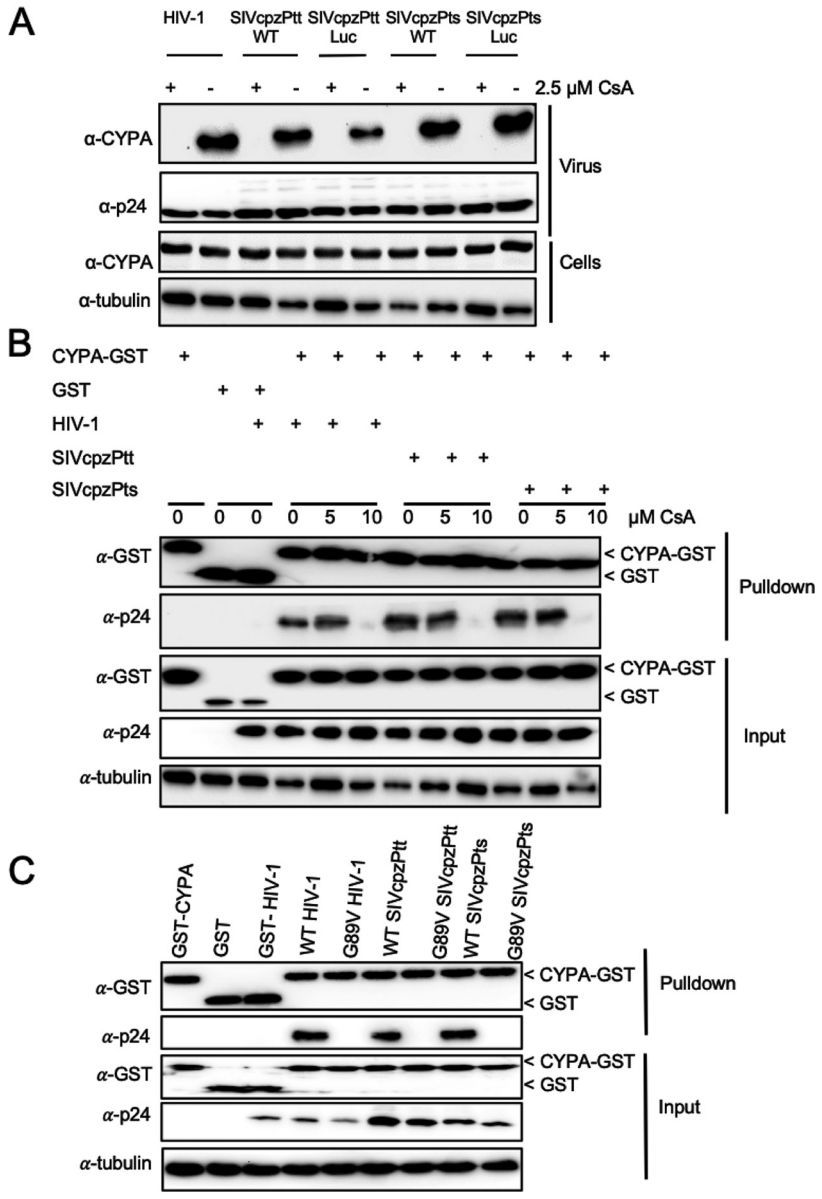

FIG 4 SIVcpz interacts with CYPA. (A) HIV-1, SIVcpzPtt, and SIVcpzPts encapsidate CYPA. Viruses were generated by the transfection of expression plasmids in HEK293T cells in the absence (−) or presence (+) of 2.5 μM CsA. SIVcpzPtt and SIVcpzPts wild-type (WT) and luciferase (Luc) reporter viruses were analyzed. Protein lysates of purified virions and HEK293T producer cells were subjected to immunoblotting. p24 (capsid) and CYPA were detected with specific antibodies. α, anti. (B) HIV-1, SIVcpzPtt, and SIVcpzPts GAGs interact with CYPA. HEK293T cells were cotransfected with HIV-1, SIVcpzPtt, or SIVcpzPts and CYPA-GST in the presence (+) or absence (−) of 5 or 10 μM CsA. Forty-eight hours later, cells and virions were lysed, and the lysate was used for pulldown experiments using GST-Sepharose beads. Proteins of cells were subjected to immunoblotting. p24 (capsid) and CYPA were detected with specific antibodies. (C) G89V in the CYPA binding loops of HIV-1, SIVcpzPtt, and SIVcpzPts capsids is important for interaction with CYPA. Similar to panel B, CYPA-GST pulldown of WT and G89V mutated viruses was performed.

Although no crystal structure information for a CPSF6/SIVcpz CA complex is available, CPSF6 likely binds at the same site in SIVcpzPts or SIVcpzPtt CA as in HIV-1 CA because of the high sequence identity between the proteins (HIV-1 CA versus SIVcpzPts CA, 79%; HIV-1 CA versus SIVcpzPtt CA, 90%) (Fig. 2A and B). The binding sites are located at the interface between two monomers, which are part of the hexameric CA structure. Although the binding sites for CPSF6 are highly similar for HIV-1 CA versus SIVcpzPtt CA (identity of 24 residues involved in CPSF6 binding, 96%), the binding sites

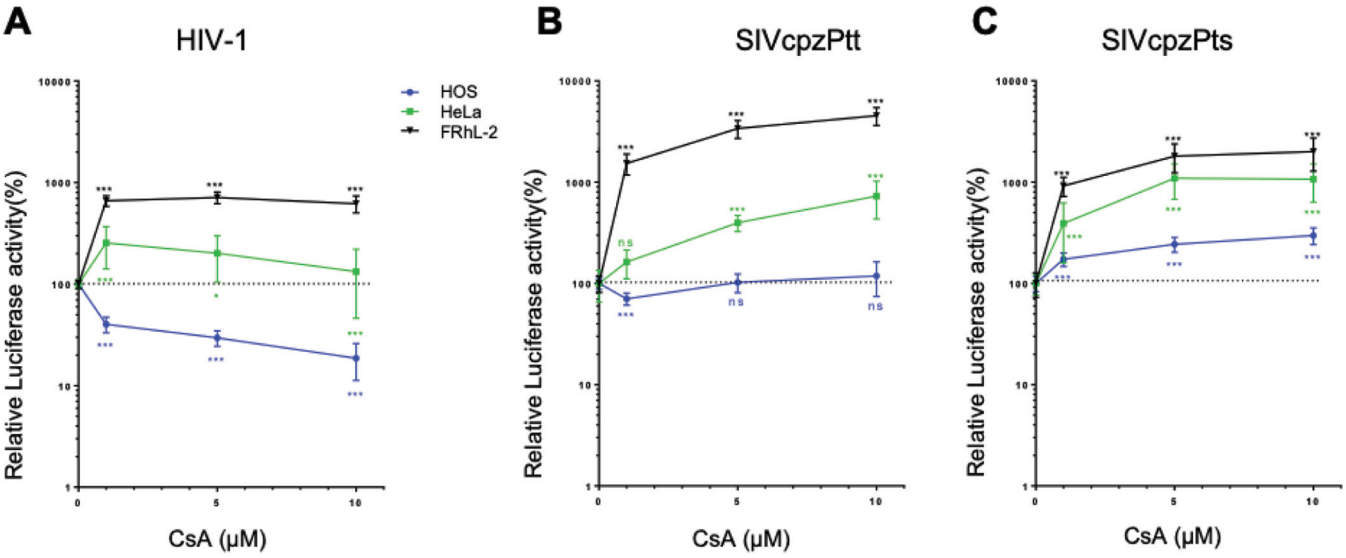

FIG 5 Infection of cells by HIV-1 or SIVcpz viruses in the presence of increasing amounts of CsA. HOS, HeLa, or FRhL-2 cells were treated with DMSO or CsA (1, 5, or 10 μM) 2 h before infection. (A) Infection by HIV-1 luciferase reporter virus. (B) Infection by SIVcpzPtt luciferase reporter virus. (C) Infection by SIVcpzPts luciferase reporter virus. Luciferase activity was measured at 2 days postinfection. Results were normalized to the DMSO control. Means and SD (error bars) are shown, and a Mann-Whitney U test was performed. Each experiment was performed three times in triplicates. ns, not significant; *, $P < 0.05$; ***, $P < 0.001$.

for HIV-1 CA versus SIVcpzPts CA are more distinct (88%) (Fig. 8A and B). To gain further insights, we generated structural models of CPFS6/CA proteins, using in all cases homology models of the CA proteins to improve their comparability. All homology models are of high structural quality, as indicated by the model quality assessment program TopScore (73) (Fig. 2C to F).

The binding site of SIVcpzPtt differs in 1 residue from HIV-1: SER178′ versus THR178′ (Fig. 8A to E). As in this case, the closest residue of CPFS6, GLN319, interacts with its N_δ with the backbone O of either serine or threonine, no impact of this substitution on CPSF6 binding is expected.

The binding site of SIVcpzPts CA differs in 3 residues from HIV-1 CA: SER102 versus ALA102, LEU172′ versus ILE175′, and ASN183′ versus THR186′ (dashed residues indicate a residue location on the second monomer; Fig. 8A to E). As residue 102 is more than 4.4 Å away from CPSF6, no direct impact on CPSF6 binding due to this substitution is expected. Residue 102 also differs within SIVcpz viruses: ALA102 and SER102 appear at equally frequencies in all investigated SIVcpz sequences (Fig. 2B). The replacement of leucine by isoleucine is a conservative one with respect to both the size of the residue and the potential interactions with CPSF6 and, hence, is not expected to influence CPSF6 binding either. Yet the replacement of asparagine by threonine may have an impact. Besides the difference in the sizes of the residues, C_γ of threonine and the phenyl ring of PHE316 of CPSF6 form a close contact that is not present in the case of asparagine. To conclude, the structural analysis of the binding mode models of CPSF6 in all three CA proteins suggests that CPSF6 binding to HIV-1 CA and SIVcpzPtt CA is similar, whereas differential binding may be expected in the case of SIVcpzPts CA. These results parallel the ones described above on the sensitivity of HIV-1 or SIV in the presence of CPSF6-358.

SIVcpz viruses, but not HIV-1, show cell type-specific sensitivity to capsid inhibitors. The unexpected observation that the nonzoonotically transmitted virus SIVcpzPts was insensitive to CYPA KO or the expression of CPSF6-358 in HOS cells motivated us to test capsid inhibitors that bind in the same capsid pocket as CPSF6 (Fig. 9A). We tested three cell lines (human HOS and HeLa and rhesus macaque FRhL-2) and compared the strong inhibitor PF74 with the less-potent variant PF57 (PF-3759857) (8) from 0.5 μM to 8 μM. HIV-1 was inhibited in all three cell lines by both inhibitors in a dose-dependent manner up to 100-fold by PF74 and up to 10-fold by PF57 (Fig. 9B and

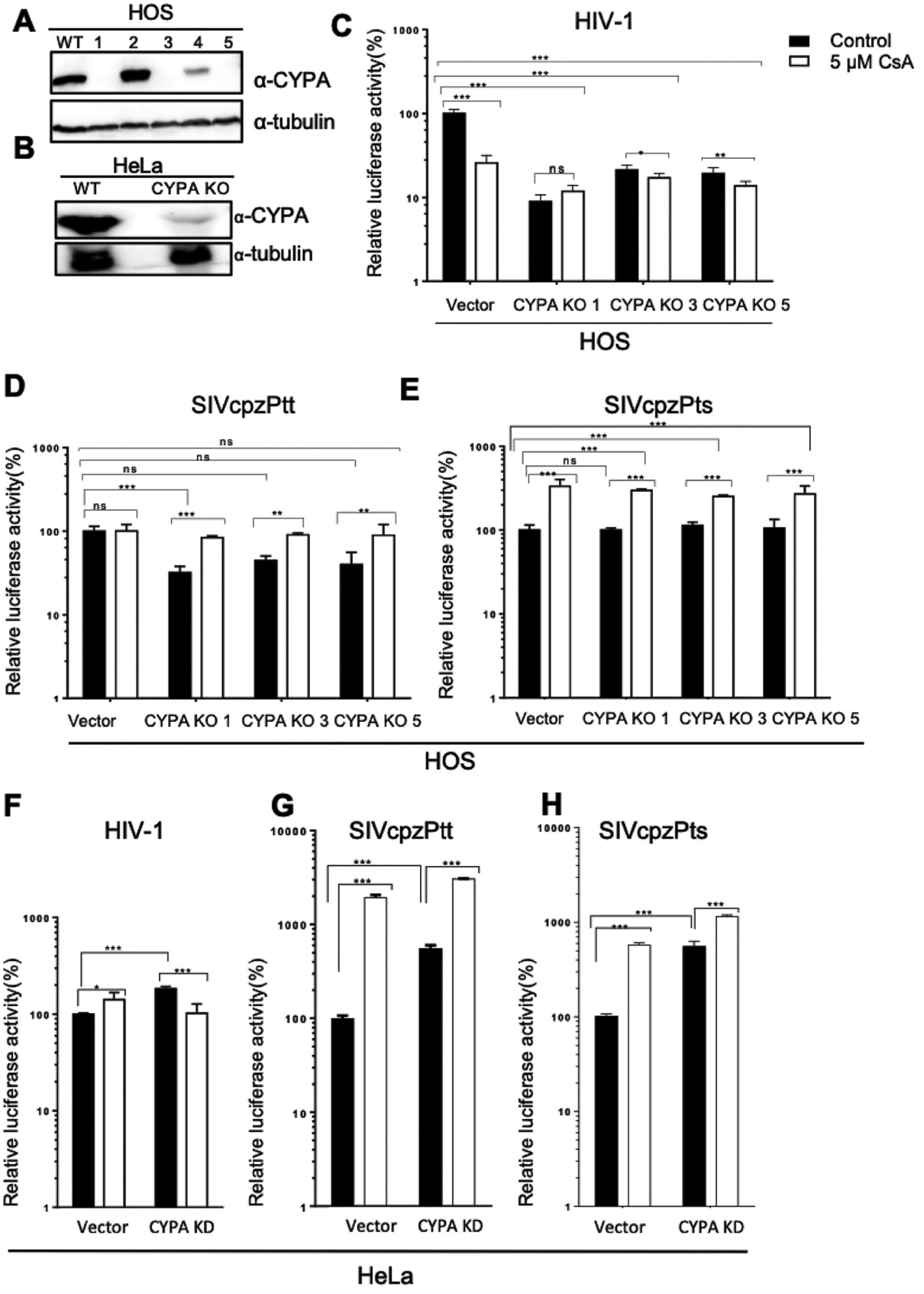

FIG 6 Infection of CYPA knockout cells by HIV-1, SIVcpzPtt, or SIVcpzPts. (A) Immunoblot of protein lysates of HOS cell clones with a CYPA knockout (KO). CYPA and tubulin were detected using specific antibodies. α, anti. (B) Immunoblot for CYPA knockdown (KD) in HeLa cells (cell

(Continued on next page)

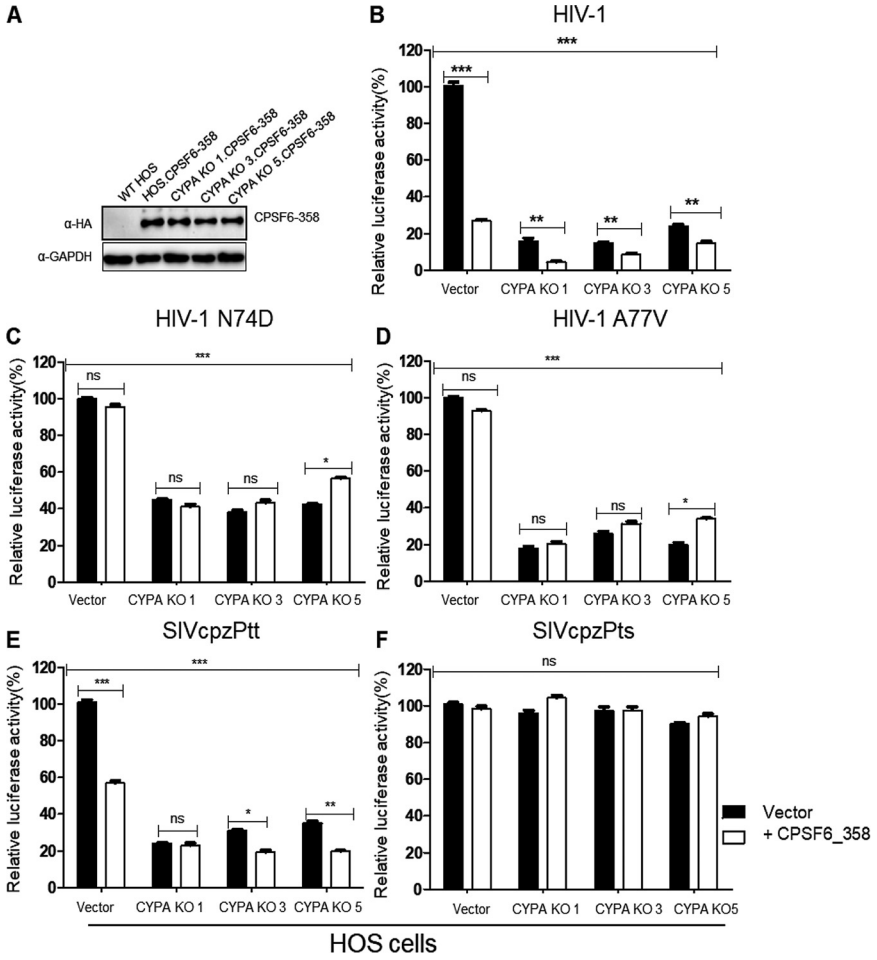

FIG 7 Infection of cells expressing CPSF6-358 by HIV-1, SIVcpzPtt, or SIVcpzPts. (A) Immunoblot of protein lysates of HOS cells for CPSF6-358 expression. HOS WT (vector pLNCX2), HOS.CPSF6-358, and HOS.CYPA KO.CPSF6-358 (clones 1, 3, and 5) cells are shown. HA-tagged CPSF6-358 and glyceraldehyde-3-phosphate dehydrogenase (GAPDH) were detected using their specific antibodies. α, anti. (B to F) Luciferase reporter viruses of HIV-1 (B), the HIV-1 A77V capsid mutant (C), the HIV-1 N74D capsid mutant (D), SIVcpzPtt (E), and SIVcpzPts (F) were used to infect HOS cells with an empty vector, HOS cells expressing CPSF6-358, CYPA KO HOS cells, or CYPA KO HOS cells expressing CPSF6-358. Luciferase activity was measured at 2 days postinfection. Results were normalized to infection in cells with the empty vector. Means and SD (error bars) are shown, and a Mann-Whitney U test was performed. Each experiment was performed three times in triplicates. ns, not significant; *, $P < 0.05$; **, $P < 0.01$; ***, $P < 0.001$.

C). Each cell line showed a slightly different dose-response curve, and the inhibitory effect of both inhibitors was strongest in FRhL-2 cells. Infection by SIVcpzPtt and SIVcpzPts was different from that by HIV-1. PF57 and PF74 inhibited both SIVcpz viruses in human HOS cells in a dose-dependent manner to levels that were comparable to those for the inhibition of HIV-1 (Fig. 9D to G). PF74 reached saturating inhibition at the lowest tested concentration for SIVcpzPtt in HeLa cells, and this inhibition was 10-fold less than that in HOS cells (Fig. 9D). PF57 at 8 μM restricted SIVcpzPtt in HeLa cells similarly to that in HOS cells, but the dose-response curves differed (Fig. 9E). Neither

FIG 6 Legend (Continued)
population). (C to E) Infection of HOS cell clones 1, 3, and 5 and HOS cells carrying an empty vector with luciferase reporter viruses of either HIV-1 (C), SIVcpzPtt (D), or SIVcpzPts (E) in the absence (DMSO control) or presence of 5 μM CsA. Luciferase activity was measured at 2 days postinfection. (F to H) Infection of HeLa cells carrying an empty vector and CYPA knockdown HeLa cells with HIV-1 (F), SIVcpzPtt (G), or SIVcpzPts (H) in the absence (DMSO control) or presence of 5 μM CsA. Results were normalized to the DMSO control in cells carrying the empty vector. Means and SD (error bars) are shown, and a Mann-Whitney U test was performed. Each experiment was performed three times in triplicates. ns, not significant; *, $P < 0.05$; **, $P < 0.01$; ***, $P < 0.001$.

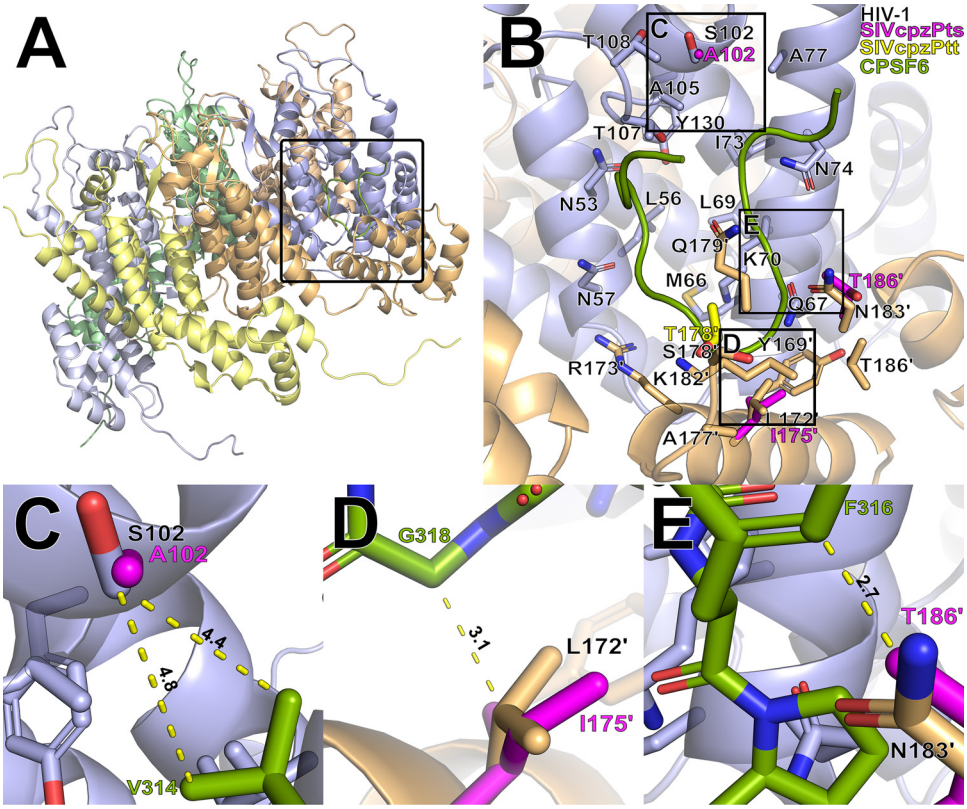

FIG 8 Binding of the CPSF6 fragment to CA hexamers. (A) Modes of binding of human CPSF6 to homology models of HIV-1 CA and SIVcpzPts/Ptt CA. For the latter two, CPSF6 coordinates were taken after superimposing the proteins onto HIV-1 CA bound to CPSF6 (PDB accession number 4WYM). Monomers are colored differently; the region in the black box is shown as a blowup in panel B, side chains of interacting residues are shown as sticks, and residues marked with dashed lines belong to a different chain. (B) The binding pockets differ in 3 residues between HIV-1 CA and SIVcpzPts CA: SER102 versus ALA102, LEU172′ versus ILE175′, and ASN183′ versus THR186′. The binding pockets differ in 1 residue between HIV-1 CA and SIVcpzPtt CA: SER178′ versus THR178′. Helix 179′–195′ is not shown. (C to E) Blowups of the regions in the black boxes in panel B. Side chains of interacting residues and the CPSF6 fragment are shown as sticks. Numbers indicate distances in angstroms.

inhibitor exhibited antiviral activity against SIVcpzPtt in the rhesus macaque FRhL-2 cell line (Fig. 9D and E). More unexpected results were obtained when testing SIVcpzPts. This virus was sensitive to capsid inhibitors in human HOS cells only but showed resistance in human HeLa and simian FRhL-2 cells (Fig. 9F and G). To rule out an effect of TRIM5α, which may be a factor that regulates viral susceptibility to capsid inhibitors, we infected feline CRFK cells that naturally lack the expression of a restricting TRIM5α protein with HIV-1 and both SIVcpz viruses (46). In CRFK cells, all three viruses were sensitive to PF74 and PF57, but SIVcpzPts was the least inhibited (Fig. 10A to C).

The recently described small-molecule HIV CA inhibitor GS-CA1 (Fig. 10D) has an antiviral activity that is >5,000-fold more potent than that of PF74 against HIV-1; both inhibitors use the same binding groove in CA (38). The use of 10 nM GS-CA1 was sufficient to inhibit HIV-1 infection of HeLa cells more than 400-fold. In comparison, SIVcpzPtt was inhibited only 16-fold and SIVcpzPts was inhibited only 3-fold by this concentration of GS-CA1 in HeLa cells (Fig. 10E to G). Despite the structural differences of PF74 and GS-CA1, SIVcpz viruses are 25- to 130-fold less sensitive to GS-CA1 than HIV-1.

To test if resistance to capsid inhibitors is also seen in primary human cells, we infected macrophages and peripheral blood mononuclear cells (PBMCs) in the presence of PF74. HIV-1 was inhibited up to 10-fold by PF74 in PMBCs and macrophages (Fig. 11A to D), while PF74 could not block infection by SIVcpzPtt and SIVcpzPts in PBMCs (Fig. 11A and B). However, in macrophages, PF74 showed some activity against SIVcpzPtt (up

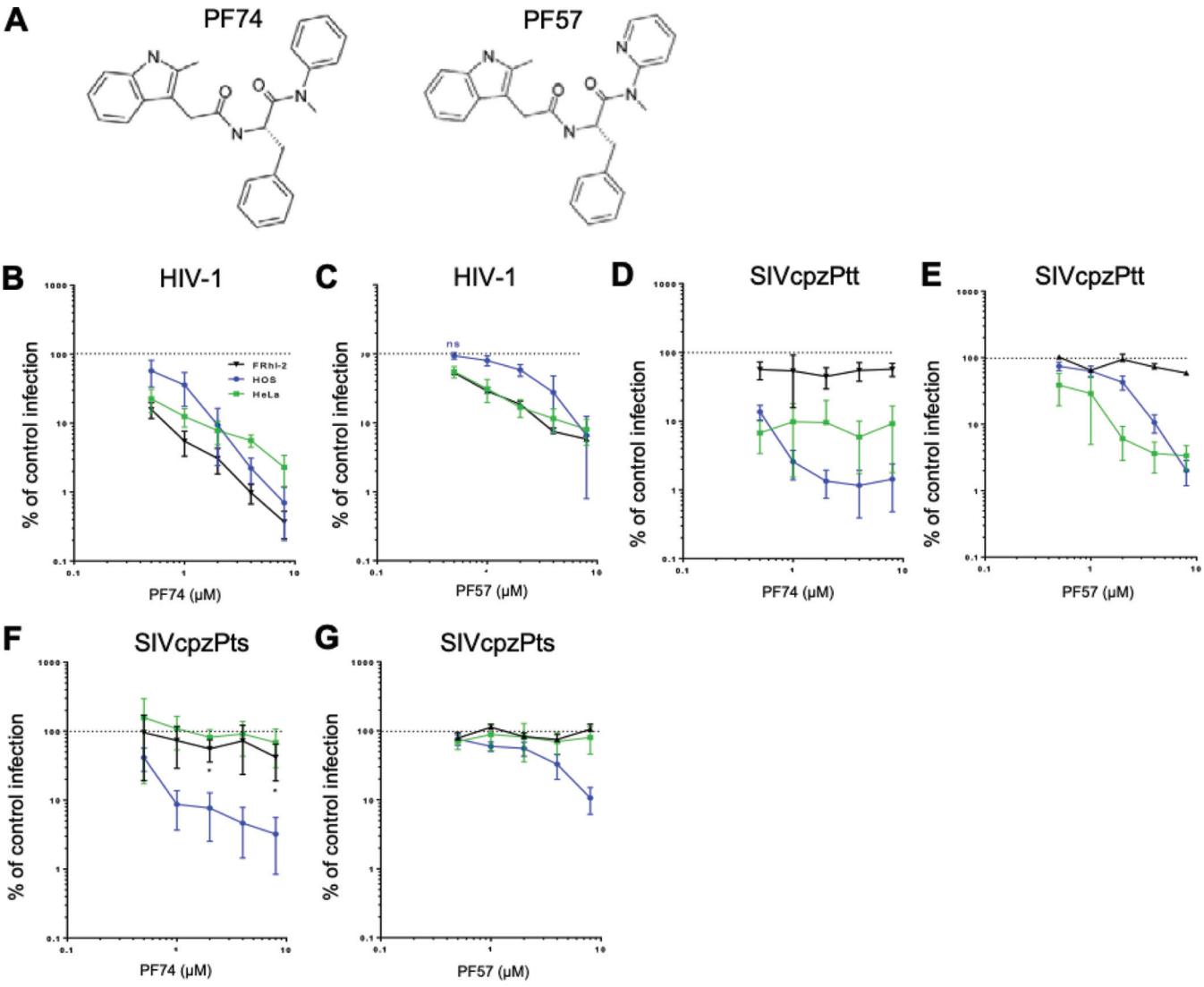

FIG 9 Infection of HOS, HeLa, or FRhL-2 cells with HIV-1, SIVcpzPtt, or SIVcpzPts in the presence of the capsid inhibitor PF57 or PF74. (A) Chemical structures of PF74 and PF57. Cells were incubated with increasing amounts of capsid inhibitors (PF57 or PF74) or DMSO for control infections. (B to G) Two hours later, cells were infected with luciferase reporter viruses of HIV-1 (B and C), SIVcpzPtt (D and E), or SIVcpzPts (F and G), and luciferase activity was measured at 2 days postinfection. Differences between control and PF74 or PF57 treatments are significant for HIV-1 in all cells ($P < 0.05$). For SIVcpzPts, differences are significant in HOS cells but not in HeLa or FRhL-2 cells; exceptions are marked with * for significant ($P < 0.05$). For SIVcpzPtt, inhibition is significant in HeLa and HOS cells. The infectivity of SIVcpzPts is significantly reduced only in HOS cells. Means and SD (error bars) are shown, and a Mann-Whitney U test was performed. Each experiment was performed at least three times in triplicates. ns, not significant.

to 2-fold inhibition) but not SIVcpzPts (Fig. 11C and D). Together, these results demonstrate that SIVcpz viruses in principle are sensitive to capsid inhibitors and that cellular factors may regulate whether these compounds can target these viruses.

Binding sites for PF74 are highly similar in the three CA proteins. In HIV-1 CA, the binding site for PF74 is also located at the interface between two monomers, as for CPSF6 (31) (Fig. 12A and B). Yet PF74 is small and interacts with only 16 residues compared to CPSF6 (Fig. 2A). Although no crystal structure information on a PF74/SIVcpz CA complex is available, PF74 likely binds at the same site in SIVcpzPts or SIVcpzPtt CA as in HIV-1 CA because of the high sequence identity between the proteins (Fig. 2A). In particular, the sites for binding or putative binding of PF74 are identical for HIV-1 CA versus SIVcpzPtt CA and highly similar for HIV-1 CA versus SIVcpzPts CA (identity of residues involved in PF74 binding, 94%) (Fig. 2A, B, D, and F and Fig. 12A and B). The putative binding site of SIVcpzPts differs in 1 residue from HIV-1: LEU172′ versus ILE175′ (Fig. 2A and B and Fig. 12A and B). As discussed above,

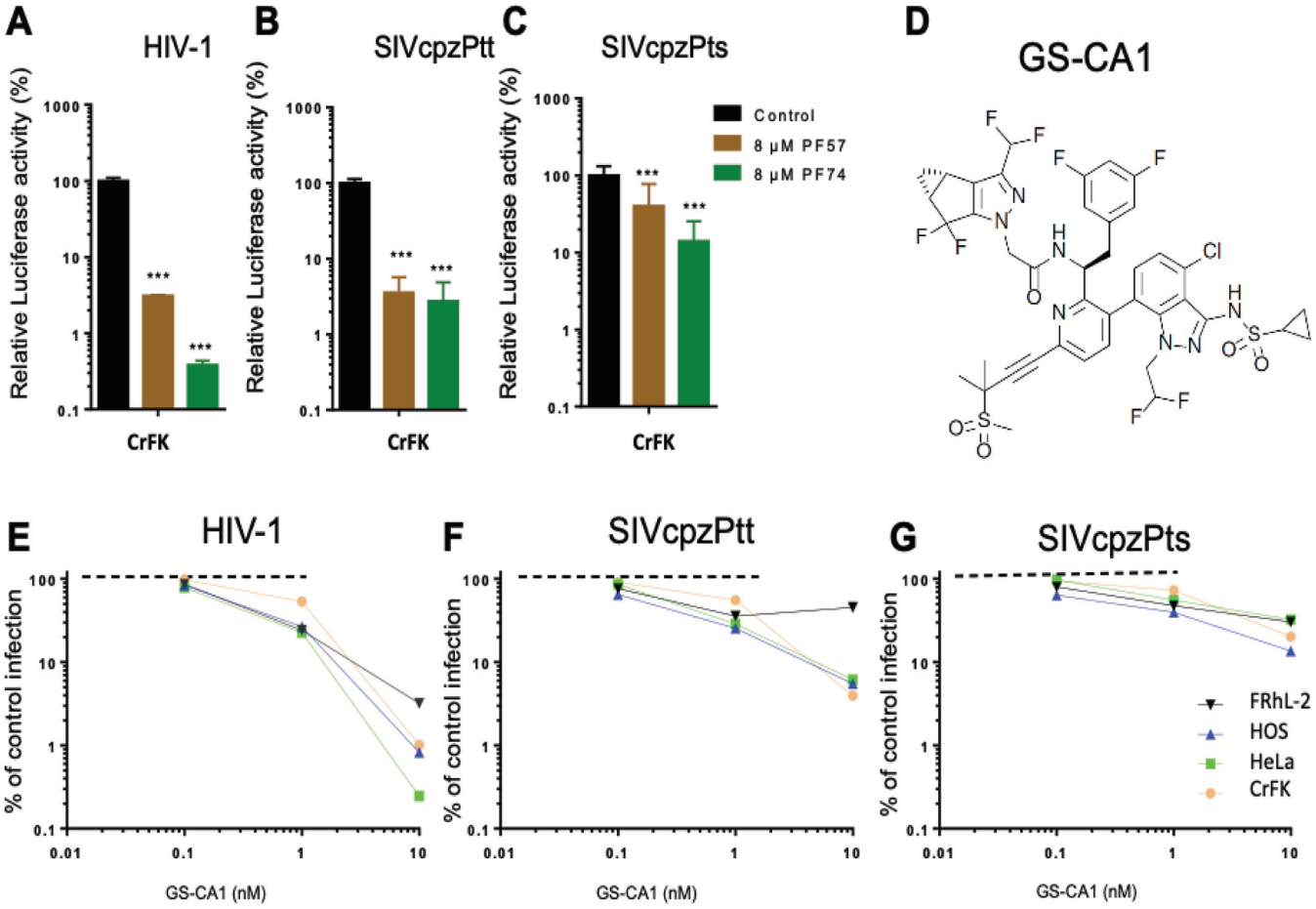

FIG 10 Infection of CRFK cells with HIV-1, SIVcpzPtt, or SIVcpzPts in the presence of the capsid inhibitor PF57 or PF74 and test of the antiviral activity of GS-CA1. (A to C) CRFK cells were incubated with capsid inhibitors (PF57 or PF74) or DMSO for control infections. Two hours later, cells were infected with luciferase reporter viruses of HIV-1 (A), SIVcpzPtt (B), or SIVcpzPts (C), and luciferase activity was measured at 2 days postinfection. Means and SD (error bars) are shown, and a Mann-Whitney U test was performed for significance. (D) Chemical structure of GS-CA1. (E to G) CRFK, HeLa, HOS, and FRhL-2 cells were incubated with the capsid inhibitor GS-CA1 or DMSO. Two hours later, cells were infected with luciferase reporter viruses of HIV-1 (E), SIVcpzPtt (F), or SIVcpzPts (G), and luciferase activity was measured at 2 days postinfection. Each experiment was performed more than three times in triplicates. ***, $P < 0.001$.

this is a conservative substitution with likely no impact on PF74 binding. To conclude, the structural analysis of the binding mode models of PF74 in all three CA proteins suggests that PF74 binding is highly similar in the three proteins.

Effective binding energies of PF74 are indistinguishable for HIV-1 and SIVcpz-Pts/Ptt CA proteins. To validate the data from the structural analysis of PF74 binding to HIV-1 and SIVcpzPts/Ptt CA proteins, we performed endpoint free energy computations using the molecular mechanics Poisson-Boltzmann (MM-PBSA) method (74) and the single-trajectory approach (75) based on five replicates of molecular dynamics (MD) simulations for each PF74/hexameric CA protein complex of 200 ns each (Fig. 12C). In all MD simulations, PF74 remained in the initial binding pose (no-fit PF74 root mean square deviations [RMSDs] of <3 Å in general, except for one binding site each in one replica each for SIVcpzPts and SIVcpzPtt [data not shown]). Furthermore, the C_α atom RMSD of binding-site residues is mostly around 1 Å (data not shown). Both results indicate that the initial starting structures of PF74 in homology models of CA proteins are plausible. The computed effective binding energies are generally stable over the simulation times and form Gaussian-shaped cumulative distributions (Fig. 12C). They mutually differ by less than 1 kcal mol^{-1} for the three PF74/CA protein complexes. As chemical accuracy is $\sim$1 kcal mol^{-1}, which is the expected accuracy in an optimal case (76), the values are thus indistinguishable from each other (Fig. 12C).

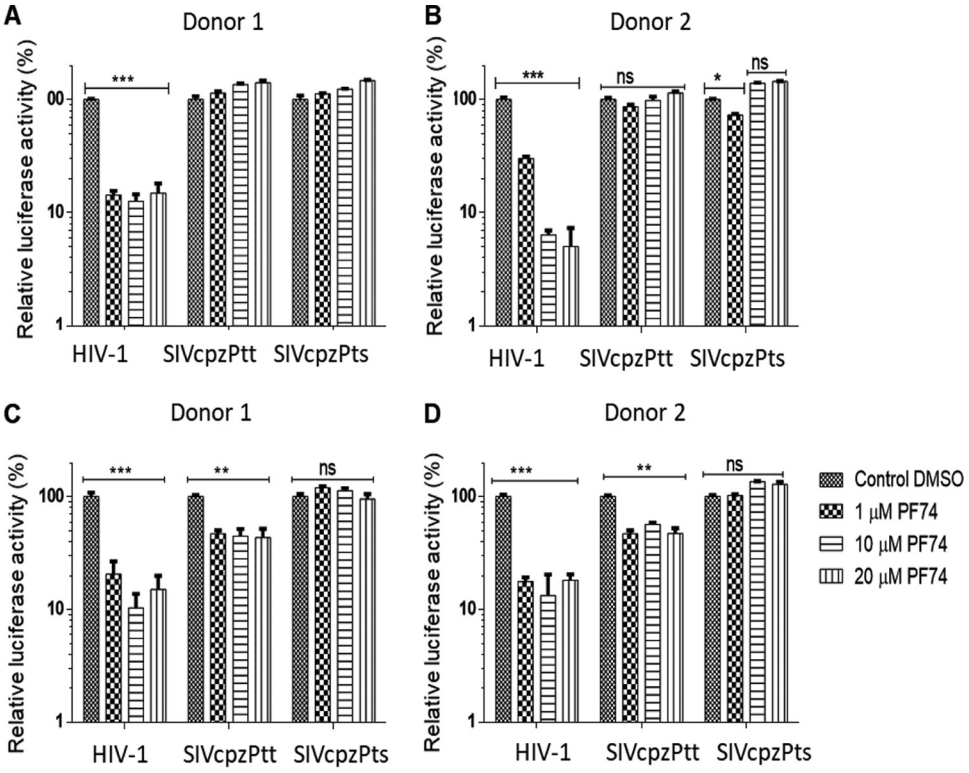

FIG 11 Infection of human PBMCs and macrophages with HIV-1, SIVcpzPtt, or SIVcpzPts in the presence of the capsid inhibitor PF74. PBMCs (A and B) and macrophages (C and D) were incubated with PF74 or DMSO and infected with luciferase reporter viruses of HIV-1, SIVcpzPtt, or SIVcpzPts. Luciferase activity was measured at 2 days postinfection. Means and SD (error bars) are shown, and a Mann-Whitney U test was performed for significance. Each experiment was performed more than three times in triplicates. ns, not significant; *, $P < 0.05$; **, $P < 0.01$; ***, $P < 0.001$.

To conclude, effective binding energy computations on PF74/CA protein complexes corroborate that PF74 binding is highly similar for the three proteins.

Cyclosporine treatment or mutations in the CYPA binding loop rescue PF74 activity against SIVcpzPts in HeLa cells. To investigate whether CsA treatment affects viral sensitivity to capsid inhibitors, drug combinations of CsA and PF74 were tested. We used PF74 either alone (1, 4, or 8 μM) or in combination with CsA (1 or 10 μM) in HeLa cells. Infections were normalized to those of cells treated with either dimethyl sulfoxide (DMSO) or CsA only to measure the inhibitory capacity of PF74. In HIV-1-infected cells, the addition of 10 μM CsA enhanced the antiviral activity of PF74 2- to 10-fold; 1 μM CsA did not change viral sensitivity to 1 μM PF74 but led to more inhibition at higher PF74 concentrations (Fig. 13A). A similar result was found in SIVcpzPtt infections, although 1 μM CsA slightly reduced inhibition by 1 μM PF74, and 10 μM CsA enhanced inhibition by 8 μM PF74 by 18-fold (Fig. 13B). Interestingly, CsA treatment changed the resistance of SIVcpzPts to PF74, and both 1 μM and 10 μM CsA enhanced the antiviral activity of higher concentrations of PF74 by 14-fold (Fig. 13C). Similar results were also obtained using PF57 (data not shown).

The finding that treatment of HeLa cells with CsA reverses the PF74 resistance of SIVcpzPts motivated us to ask if capsid binding to CYPA is important for this phenotype. For these experiments, we used viruses that carry the G89V mutation in the capsid loop that interacts with CYPA. The HIV-1 G89V mutant together with a low concentration of PF74 had 2-fold-higher sensitivity, but PF74 concentrations above 1 μM inhibited HIV-1 WT and G89V equally (Fig. 13D). PF74 had 5- to10-fold-increased antiviral activity against SIVcpzPtt G89V compared to the WT virus (Fig. 13E). Strikingly, the mostly PF74-resistant virus, SIVcpzPts, was completely sensitive to the capsid inhibitor, with up to 50-fold inhibition, when mutated to G89V in CA (Fig. 13F). Infections by HIV-1 and

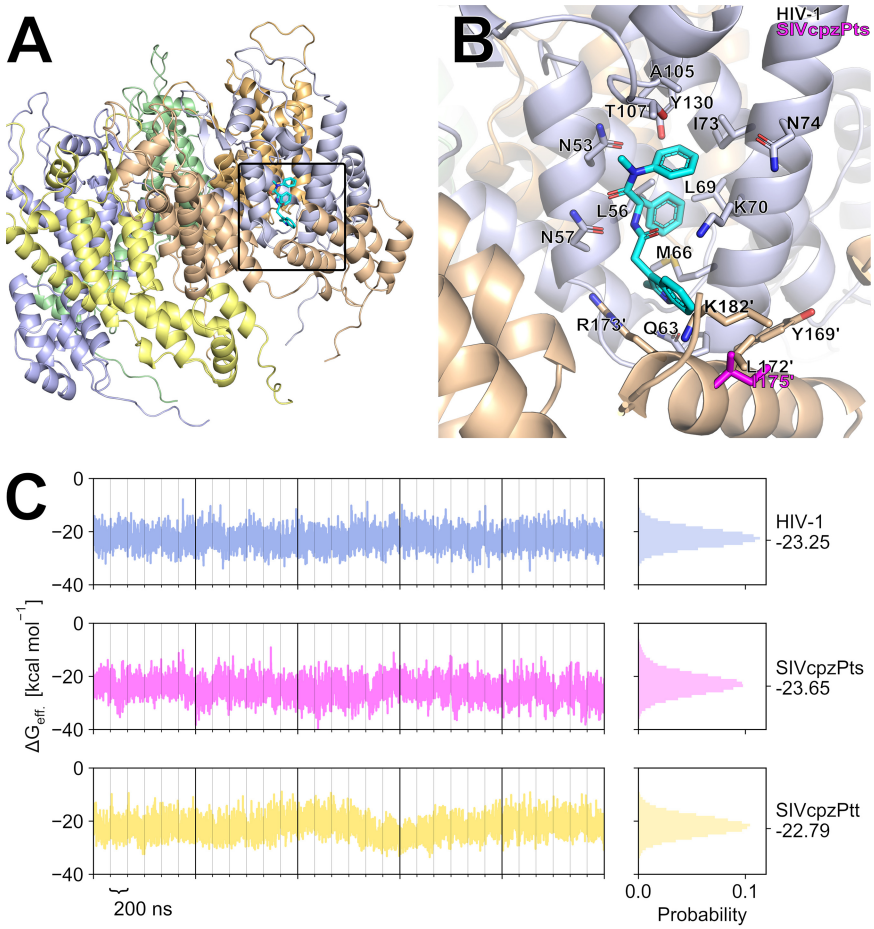

FIG 12 Binding of PF74 to CA hexamers. (A and B) Modes of binding of PF74 to homology models of HIV-1 CA and SIVcpzPts/Ptt CA proteins. For the latter two, PF74 coordinates were taken after superimposing the proteins onto HIV-1 CA bound to PF74 (PDB accession number 4XFZ). Monomers are colored differently; the region in the black box in panel A is shown as a blowup in panel B, side chains of interacting residues are shown as sticks, and residues marked with dashed lines belong to a different chain. The binding pockets differ in 1 residue between HIV-1 CA and SIVcpzPts CA: LEU172′ versus ILE175′. The binding pockets of HIV-1 CA and SIVcpzPtt CA do not differ. Helix 179′–195′ is not shown in panel B. (C) Effective binding energies computed by the molecular mechanics Poisson-Boltzmann surface area (MM-PBSA) method. Shown are the effective binding energies of PF74 binding to HIV-1 (blue), SIVcpzPts (pink), and SIVcpzPtt (yellow) CA proteins as a function of the simulation time (left). Values per trajectory are separated by black vertical lines, and gray lines separate values computed for each binding site of a CA hexamer. On the right, the probability functions of the effective energies across all frames are shown. The average effective binding energy for each isoform is marked on the right axis. The standard error of the mean (see the equation in Materials and Methods) is <0.015 kcal mol^{-1} in all cases.

SIVcpz WT and G89V viruses in the presence of GS-CA1 generated similar results for HIV-1 and SIVcpzPtt, but the moderate inhibition of SIVcpzPts was enhanced only 5-fold by the G89V mutation (Fig. 13G to I). Our findings suggest that an important regulator of the antiviral activity of PF74-like capsid inhibitors is a CsA-sensitive protein, which is likely the SIVcpz capsid-interacting protein CYPA.

Cyclophilin A knockout overcomes the resistance of SIVcpzPts to capsid inhibitors in HeLa cells. To test whether the presence of CYPA in viral target cells protects SIVcpzPts against capsid inhibitors, HeLa.CYPA KD and HOS.CYPA KO (clone 3) cells were infected in the presence of increasing amounts of PF74 or PF57. For HeLa.CYPA KD cells compared to WT cells, HIV-1 was less inhibited by lower concentrations of PF74 and similarly inhibited at higher concentrations (Fig. 14A), which is similar to previously described results (33). In contrast, PF57 showed reduced activity against HIV-1 in HeLa.CYPA KD cells compared to WT cells at all drug concentrations (Fig. 14B). This

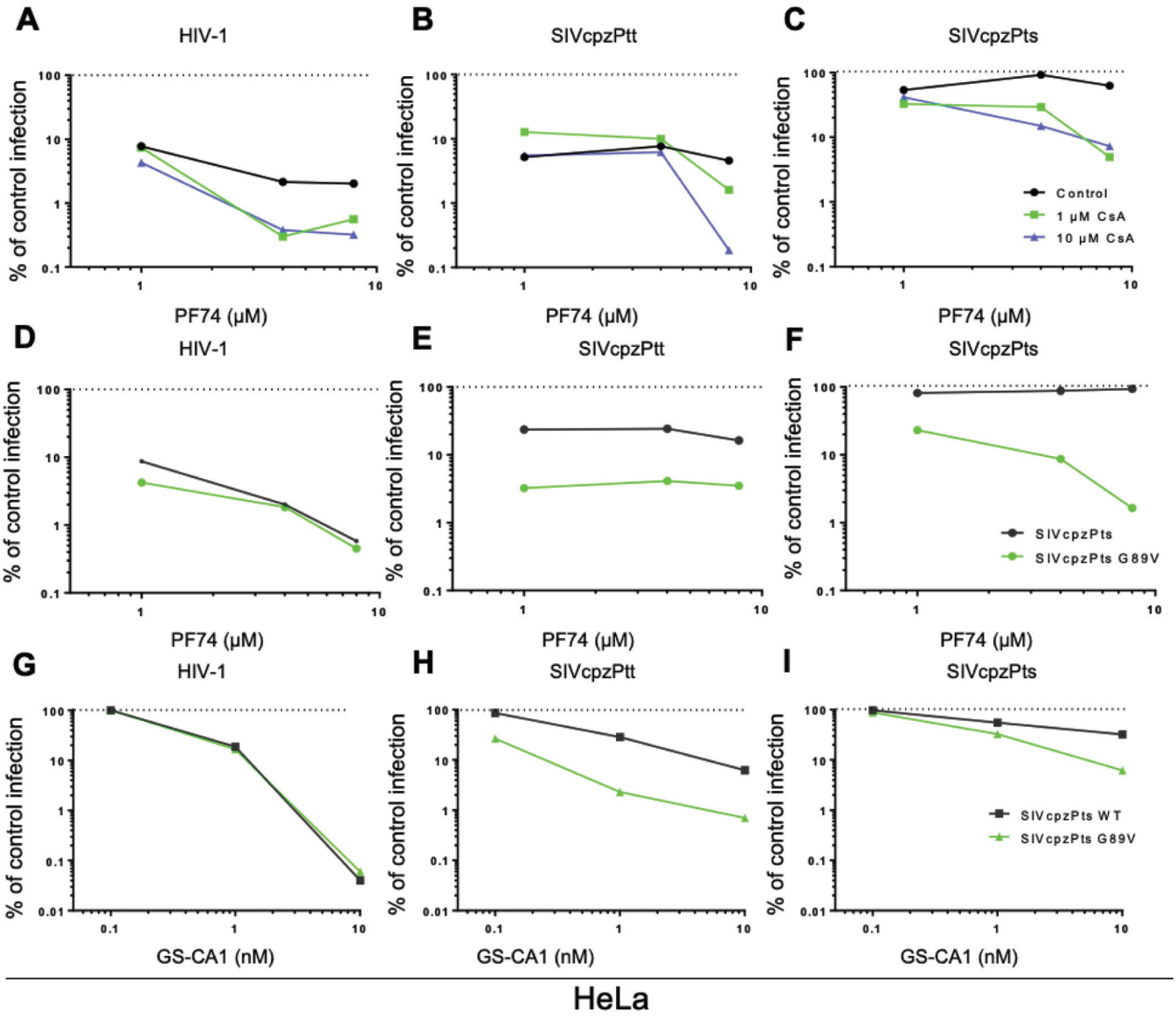

FIG 13 Infection of HeLa cells in the presence of CsA or infection with CYPA loop mutants (G89V) in the presence of capsid inhibitors. (A to C) HeLa cells were incubated with 1, 4, or 8 μM the capsid inhibitor PF74, DMSO, or the capsid inhibitor together with CsA (1 or 10 μM). Two hours later, cells were infected with luciferase reporter viruses of HIV-1 (A), SIVcpzPtt (B), or SIVcpzPts (C), and luciferase activity was measured at 2 days postinfection. Results were normalized to infection of cells treated with DMSO (control) or cells treated with CsA only. (D to I) Infection of HeLa cells with CYPA loop mutants (G89V) of HIV-1, SIVcpzPtt, or SIVcpzPts in the presence of capsid inhibitors. Cells were incubated with increasing amounts of the capsid inhibitor PF74 (D to F) or GS-CA1 (G to I) or with DMSO for control infections. Two hours later, cells were infected with luciferase reporter viruses of HIV-1 and HIV-1 G89V (D and G), SIVcpzPtt and SIVcpzPtt G89V (E and H), and SIVcpzPts and SIVcpzPts G89V (F and I). Luciferase activity was measured at 2 days postinfection. Results were normalized to infection of cells treated with DMSO. Each experiment was performed three times in triplicates.

pattern of inhibition was also seen in HOS.CYPA KO cells for HIV-1 (Fig. 14C and D) and SIVcpzPtt (Fig. 14G and H) treated with PF74 and PF57 and for SIVcpzPts treated with PF57 (Fig. 14L). PF74 inhibited SIVcpzPts in HOS.CYPA KO cells compared to WT cells, with reduced activity at low concentrations and higher inhibition at increased drug concentrations (Fig. 14K).

HeLa.CYPA KD cells infected with the SIVcpz viruses displayed two further inhibition curves. CYPA KD in HeLa cells minimally (<2-fold) enhanced PF74 activity but did not change PF57 activity against SIVcpzPtt (Fig. 14E and F). SIVcpzPts demonstrated the expected resistance to both capsid inhibitors in WT HeLa cells, but this resistance was completely lost in HeLa.CYPA KD cells (Fig. 14I and J), suggesting that in HeLa cells, CYPA is an antagonist of capsid inhibitors for SIVcpzPts.

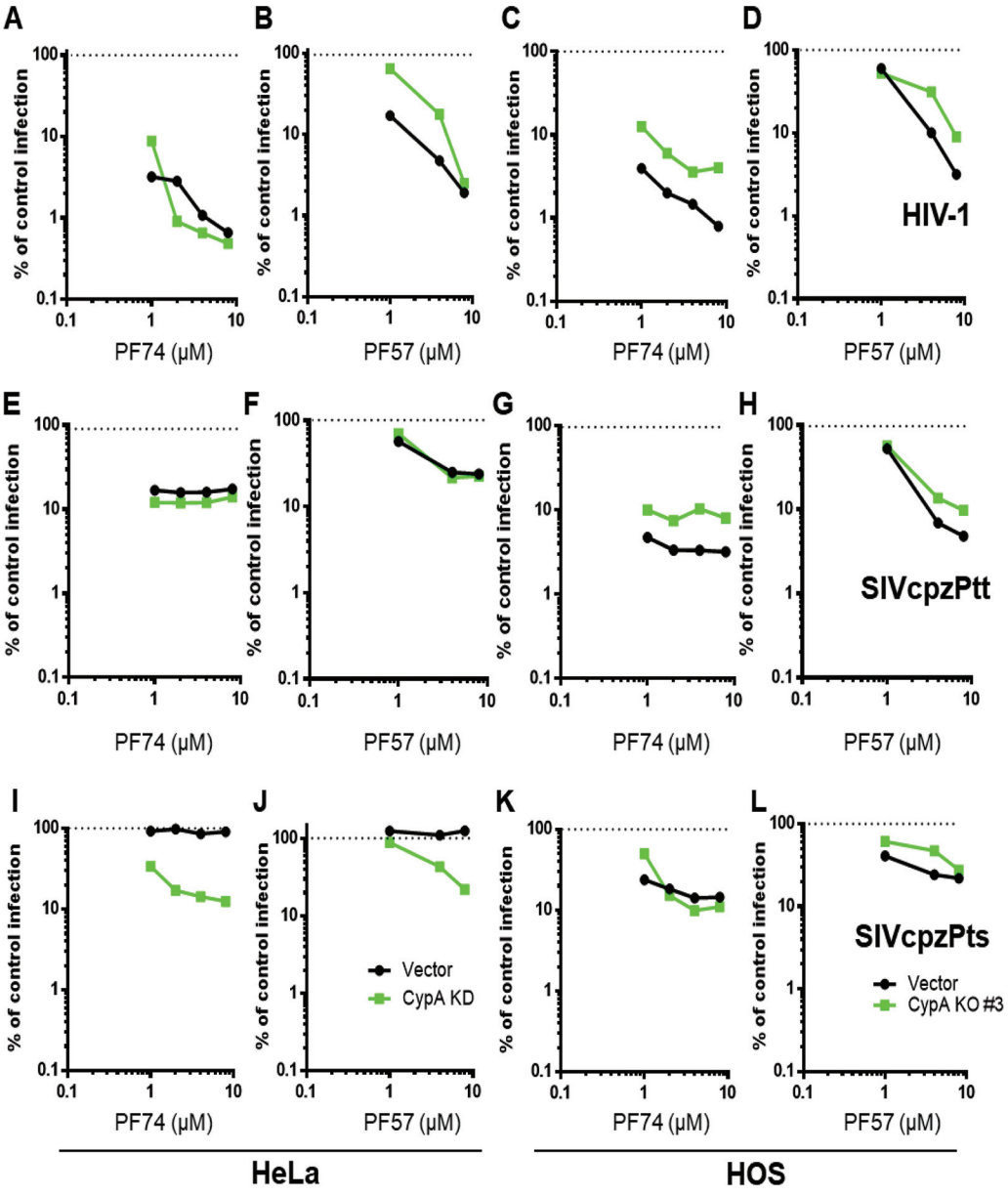

FIG 14 Infection of CYPA-KO cells with HIV-1, SIVcpzPtt, or SIVcpzPts in the presence of capsid inhibitors. HOS.CYPA KO and HeLa.CYPA KD cells were incubated with increasing amounts of capsid inhibitors (PF57 or PF74) or DMSO for control infections. Two hours later, cells were infected with luciferase reporter viruses of HIV-1 (A to D), SIVcpzPtt (E to H), or SIVcpzPts (I to L), and luciferase activity was measured at 2 days postinfection. Results were normalized to infection of cells treated with DMSO. Each experiment was performed three times in triplicates.

DISCUSSION

During the early phase of HIV-1 infection, capsid inhibitors such as PF74 either stabilize or disintegrate the core, depending on the concentrations applied (31, 32, 77, 78). The mechanism of inhibition by capsid inhibitors is currently poorly defined. Cyclophilin A was found to enhance the antiviral activity of PF74 but also to protect HIV-1 against high concentrations of PF74 (32, 33). The CYPA binding loop in the capsid does not overlap the PF74 binding site (Fig. 2A and Fig. 3), and thus, a model of how CYPA regulates PF74 activity is not straightforward. However, the binding site of PF74 in the assembled capsid hexamers and pentamers overlaps the binding sites of the cellular cofactors CPSF6 and NUP153, implicating a competition of PF74 and these cellular cofactors for the same binding groove (19, 29, 30, 33, 35, 78–80).

While the CYPA interaction with HIV-1 affects many different aspects of HIV-1 biology (18, 32, 51–60), recent studies concluded that the pathway most affected by CYPA inhibition in cell lines is viral nuclear entry (61, 81). By comparing the permissivities of human cells to SIVs of chimpanzees, we found that HeLa cells are much less permissive to these viruses than HOS cells. Treating HeLa cells with CsA or using CYPA KD HeLa cells reverted the reduced permissiveness to SIVcpz. Our data on the CYPA-capsid interaction collectively suggest that HIV-1 and SIVcpz GAG proteins interact with CYPA similarly despite differences in their CYPA binding loops. In addition to CYPA, we tested the sensitivities of the two SIVcpz viruses to the anti-HIV-1 factors CPSF6-358, PF74, and PF57 as well as the potent capsid inhibitor GS-CA1. The expression of truncated CPSF6 in the form of CPSF6-358 in human HOS cells repressed HIV-1 infections, which is consistent with previous observations (17, 33, 54, 82–84). Similarly, but more moderately, CPSF6-358 reduced the infectivity of SIVcpzPtt. However, SIVcpzPts escaped restriction by CPSF6-358 in HOS WT and in CYPA KO cells. Employing binding mode models of CPSF6 bound to all three CA proteins revealed that CPSF6 binding to HIV-1 CA and SIVcpzPtt CA is similar, whereas differential binding may be expected in the case of SIVcpzPts CA. These results parallel experimental ones in that HIV-1 and SIVcpzPtt, but not SIVcpzPts, were inhibited by CPSF6-358 expression.

The investigation of PF74 and related capsid inhibitors (PF57 and GS-CA1) confirmed that SIVcpz and HIV-1 have intrinsic biological differences that have not been observed previously. These three viruses respond differently to capsid inhibitors in a cell type-dependent manner. HIV-1 was sensitive to PF57, PF74, and GS-CA1 and was inhibited 250- to 500-fold in HOS, HeLa, FRhL-2, and CRFK cells. SIVcpz viruses showed similar sensitivities only in HOS and CRFK cells; in addition, SIVcpzPtt was sensitive to capsid inhibitors in HeLa cells. However, both SIVcpz viruses showed resistance in FRhL-2 cells and were inhibited only 2-fold at the maximum drug concentration; in addition, SIVcpzPts was resistant in HeLa cells. Importantly, the capsid inhibitors were also inactive against SIVcpzPts in human macrophages and PBMCs, and against SIVcpzPtt in PBMCs, while SIVcpzPtt was partially (2-fold) sensitive in macrophages.

Because SIVcpz viruses are not generally resistant to this type of inhibitor, we concluded that the antiviral activity of the capsid inhibitors depends on cellular infection pathways or the specific binding of a cellular protein. In particular, the finding that PF74 cannot interfere with SIVcpz infection in human PBMCs suggests that the results obtained with the cell lines are of biological relevance. Structural modeling of the PF74 interaction with CA proteins revealed that the binding sites are identical in HIV-1 CA versus SIVcpzPtt CA and highly similar for HIV-1 CA versus SIVcpzPts, suggesting that binding is highly similar for the three proteins. This suggestion was corroborated by effective binding energy computations, which are indistinguishable within chemical accuracy. These results are consistent with the similar sensitivities of all three viruses to PF74 in human HOS cells.

The PF74 inhibition curve for HIV-1 in HeLa cells was described as being triphasic, with two inhibitory phases flanking a plateau phase (19, 29, 33, 60). Here, we identified that the PF74 inhibition curve for HIV-1 in HeLa cells is only one of several different inhibition curves that capsid inhibitors can generate. Moreover, by testing capsid inhibitors against HIV-1, SIVcpzPtt, and SIVcpzPts in CsA-treated cells or in cells with CYPA KO or deficiency, we obtained a complex interaction pattern that suggests that in some cell types, and specifically for SIVcpzPts, CYPA is an important antagonist of PF74-type capsid inhibitors. Our results in HeLa cells demonstrate that the functional inactivation of CYPA by CsA at low PF74 concentrations differentially affects the antiviral activity of the capsid inhibitors. However, at high PF74 levels, CsA treatment reverted the resistance of SIVcpzPts to PF74 and further enhanced the sensitivities of HIV-1 and SIVcpzPtt. We also tested how SIVcpz and HIV-1 reacted to capsid inhibitors in HOS.CYPA KO and HeLa.CYPA KD cells. The virus inhibition curves of PF57 or PF74 in HOS or HeLa cells lacking CYPA showed either no change, 2- to 4-fold-lower antiviral activity, or slightly enhanced inhibition. The most striking observation was the total loss of resistance of SIVcpzPts to capsid inhibitors in HeLa cells due to CYPA KD. SIVcpzPts

also lost its resistance to PF74 in HeLa cells when the virus was mutated in the CYPA binding loop. This G89V mutation did not affect the sensitivity of HIV-1 to PF74 but further increased PF74's antiviral activity against SIVcpzPtt. These data suggest a diverse and elaborate pattern of regulation of antiviral capsid inhibitor activity by CYPA. However, in HeLa cells, CYPA has a clear protective role for SIVcpzPts against PF74 and PF57 at all drug concentrations.

The activity of PF74 and related compounds likely depends on the nuclear import of HIV-1 via NUP153, NUP358, and CPSF6 (1, 17–19, 33). HIV-1 variants that are more resistant to PF74's antiviral activity, but still bind the drug, are less dependent on NUP153 utilization (32, 33, 80). Knockdown of NUP153 in HeLa and HOS cells caused a 10-fold-reduced capacity of PF74 to inhibit HIV-1, with residual antiviral activity at high drug concentrations (19, 33). The knockdown of CPSF6 did not affect antiviral activity at high concentrations of PF74 but reduced the antiviral activity of the capsid inhibitor when applied at lower concentrations (33). These data, together with our findings, lead us to postulate that SIVcpz viruses, in particular SIVcpzPts, infect at least some cell types via a pathway that is independent of NUP153, NUP358, and CPSF6, consistent with recent findings describing a heterogeneity of nuclear pore complexes influencing HIV-1 infection (6, 85). We further speculate that during SIVcpz adaptation to humans, the capacity to use alternative nuclear entry pathways was lost for unknown reasons. Whether the nuclear entry pathway of SIVcpz viruses that can escape PF74 inhibition involves CYPA or CPSF6 requires further study.

MATERIALS AND METHODS

Plasmids. The murine leukemia virus (MLV) packaging construct pHIT60, which carries *gag-pol* of Moloney MLV, was provided by Jonathan Stoye (86). SIVcpzPts clone TAN1.910 (87) (GenBank accession number AF447763) was obtained from the NIH AIDS Reagent Program (Germantown, MD, USA). SIVcpzPtt clone MB897 (88) (GenBank accession number JN835461) was kindly provided by Frank Kirchhoff. The HIV-1 vector pSIN.PPT.CMV.Luc.IRES.GFP expresses firefly luciferase and green fluorescent protein (GFP) (89). The HIV-1 construct psPAX2 was obtained from the NIH AIDS Reagent Program (catalog number 11348), and pRSV-Rev, pMDLg/pRRE, and pMD.G (VSV-G) were described previously (90). HIV-1 capsid mutants were produced as follows. Using fusion PCR, the region flanking Eco72I (PmlI) and MunI (MfeI) in pMDLg/pRRE was amplified at the same time, introducing a G89V (56), N74D (54), or A77V (72) mutation in the capsid, and cloned into the pMDLg/pRRE plasmid digested by Eco72I (PmlI) and MunI (MfeI) (Thermo Fischer Scientific, Langenselbold, Germany). Using fusion PCR, the SIVcpzPtt region flanking SacII and AleI (Thermo Fischer Scientific) and the SIVcpzPts region between the NruI and BoxI (Thermo Fischer Scientific) restriction sites were amplified with the introduction of the G89V mutation into the capsids. Sequencing confirmed the desired mutations. This approach generated pMDLg/pRRE.G89V, pMDLg/pRRE.N74D, and pMDLg/pRRE.A77V HIV-1 but also SIVcpzPtt.nanoluciferase.G89V and SIVcpzPts.nanoluciferase.G89V CA mutants. To generate GST-tagged human CYPA, CYPA cDNA with HindIII and BamHI sites was cloned into the GST-containing pkMyc vector digested with the same enzymes (Thermo Fisher Scientific) to generate pkMyc.CYPA.GST. SIVcpzPtt MB897-nanoluciferase and SIVcpzPts TAN1-nanoluciferase were described previously (42). To generate pLNCX2.CPSF6-358, NotI- and XhoI-digested hemagglutinin (HA)-tagged CPSF6-358 cDNA (from plasmid LPCK-CPSF6-358.HA [17], a gift of Thomas Gramberg) was cloned into pLNCX2 (TaKaRa Bio Europe, Saint-Germain-en-Laye, France) digested with same restriction enzymes, and positive clones were confirmed by sequencing.

Cells. Wild-type HOS (ATCC CRL-1543; LGC Standards GmbH, Wesel, Germany), HeLa (ATCC CCL-2), HEK293T (ATCC CRL3216), OMK (637-69; ECACC, Sigma-Aldrich Chemie GmbH, Taufkirchen, Germany), CV-1 (ATCC CCL-70), CRFK (ATCC CCL-94), and FRhL-2 (ATCCR CL-160) cells were maintained in Dulbecco's modified Eagle's medium (Pan-Biotech, Aidenbach, Germany) supplemented with 10% fetal bovine serum (FBS), 2 mM L-glutamine, and 100 U/ml penicillin-streptomycin at 37°C in a humidified atmosphere of 5% CO_2. For HOS and HeLa CYPA knockout cells, 2 μg/ml puromycin was added to the culture medium for selection. HOS cells expressing CPSF6-358 were selected under 300 μg/ml Geneticin (Biochrom GmbH, Berlin, Germany). Human PBMCs and macrophages were isolated from whole blood, obtained from the university hospital of Heinrich Heine University Düsseldorf (ethical approval study number 3180). PBMCs were cultured in RPMI 1640 supplemented with 10 μg phytohemagglutinin (PHA) and later with 30 U/ml interleukin-2, and macrophages were maintained in RPMI 1640 containing 1,000 U/ml monocyte colony-stimulating factor (M-CSF).

HIV-1 and SIVcpz reporter viral particle production. HIV-1 VSV-G-pseudotyped viral particles were produced in a six-well plate by the transfection of HEK293T cells with 200 ng of pMD.G, 800 ng of pSIN.PPT.CMV.Luc.IRES.GFP, 350 ng of pRSV-Rev, and 800 ng of pMDLg/pRRE wild type, pMDLg/pRRE.N74D, or pMDLg/pRRE.A77V. To produce SIVcpzPtt-nanoluciferase or SIVcpzPts-nanoluciferase viruses, 2,250 ng of either reporter plasmid plus 200 ng pMD.G were used to transfect HEK293T cells. Forty-eight hours following transfection, the supernatants were collected and centrifuged for 5 min at 5,000 rpm at 4°C to pellet possible cells. Where needed, the reverse transcriptase (RT) activity of viruses was quantified using the Cavidi HS lenti RT kit (Cavidi Tech, Uppsala, Sweden).

Generation of CYPA knockout cells. The pLentiCRISPRv2 plasmid construct for CYPA knockout was constructed according to previously described protocols (91–93). Complementary oligonucleotides (5′-CACCGTTCTTCGACATTGCCGTCGA-3′ and 5′-AAACTCGACGGCAATGTCGAAGAA-3′ for HeLa cells; 5′-CACCGGACAAGGTCCCAAAGACAGC-3′ and 5′-AAACGCTGTCTTTGGGACCTTGTCC-3′ for HOS cells) containing the specific human CYPA single guide RNA (sgRNA) sequences were ligated into BsmBI-digested pLentiCRISPRv2 to generate the functional transfer vector. The LentiCRISPRv2 plasmid lacking an sgRNA sequence was used as the empty vector control. Transfection of HEK293T cells with the pLentiCRISPRv2 transfer vector containing CYPA knockout sgRNA, packaging plasmid psPAX2, and a VSV-G plasmid generated VSV-G-pseudotyped viral particles, which were used to transduce HeLa or HOS cells for 3 days. Transduced cells were then selected under 2 μg/ml puromycin. While this process almost completely removed CYPA in HeLa cells, it only reduced the protein in HOS cells. Using flow cytometry (FACSAria III sorter; BD, Heidelberg, Germany), single HOS cells with anti-CYPA constructs were isolated in wells of a 96-well plate for single clones. Gene knockout or knockdown in cell pools and clones was confirmed by immunoblotting.

Generation of CPSF6-358-expressing cells. A total of 1,150 ng of the pLNCX2.CPSF6-358 construct together with 1,150 ng of pHIT60 and 200 ng of pMD.G were used to produce gammaretroviral particles in HEK293T cells, and these particles were used to transduce wild-type or CYPA knockout HOS cells for the expression of CPSF6-358.HA. HOS cells expressing CPSF6-358 were selected using 300 μg/ml Geneticin (Biochrom GmbH). CPSF6-358 protein expression was analyzed by immunoblotting. Cells expressing the empty pLNCX2 or LentiCRISPRv2 vector were used as controls.

Single-round infection. A total of 10×10^3 cells were seeded into 96-well plates, and infection was performed the following day. PF-3450074 (PF74) (8) (Aobious Biotrend, Cologne, Germany), GS-CA1 (a gift of Gilead Sciences, Foster City, CA, USA), cyclosporine (CsA; Sigma-Aldrich), or PF-3759857 (PF57) (8) was added to cells 2 h before infection, and control infections were performed with DMSO. PF57 was obtained in two steps starting from *N*-Boc (butoxycarbonyl)-L-phenylalanine. After 48 to 72 h, firefly luciferase activity was measured with the Steady-Glo luciferase system (Promega, Mannheim, Germany), according to the manufacturer's instructions, on a MicroLumat Plus luminometer (Berthold Detection Systems, Pforzheim, Germany). For SIVcpz-nanoluciferase, cells were washed with phosphate-buffered saline (PBS) three times 48 h after infection, before lysis and luciferase measurement, in addition to a medium change 24 h following infection, to eliminate the effect of extracellular nanoluciferase on the supernatant. Nanoluciferase activity was measured with the Nano-Glo luciferase system (Promega) on a MicroLumat Plus luminometer (Berthold Detection Systems). Each experiment was performed in triplicates and at least three times.

Cyclophilin A encapsidation. HEK293T cells were seeded into 6-well plates (10^6 cells per well) 1 day before transfection. Two hours before transfection, 2.5 μM CsA or DMSO for controls was added to cells. Transfection was done as follows. Lipofectamine 2000 (Thermo Fisher Scientific) (according to the manufacturer's instructions) was used to complex a total of 2,500 ng of plasmid DNA for delivery into cells. For SIVcpz, 2,300 ng of the viral reporter plasmid and 200 ng pMD.G VSV-G were used. In the case of HIV-1, 200 ng of pMD.G, 975 ng of pSIN.PPT.CMV.Luc.IRES.GFP, 350 ng of pRSV-Rev, and 975 ng of pMDLg/pRRE were used for transfection. At 48 h posttransfection, the supernatant was collected, viral concentration was done through 20% sucrose for 4 h at 4°C, and viral pellets were lysed using Western blot lysis buffer.

Pulldown experiments. HEK293T cells were seeded into 6-well plates (10^6 cells per well) 1 day before transfection. Transfection was done as follows. Lipofectamine 2000 (Thermo Fisher Scientific) was used to complex a total of 2,600 ng of plasmid DNA for delivery into cells. For SIVcpz, 1,700 ng of the viral reporter plasmid, 200 ng of pMD.G VSV-G, and 700 ng of pcMyc.CYPA.GST constituted a plasmid complex for transfection. For HIV-1, 200 ng of pMD.G, 700 ng of pSIN.PPT.CMV.Luc.IRES.GFP, 300 ng of pRSV-Rev, 700 ng of pMDLg/pRRE, and 700 ng of pcMyc.CYPA.GST or 700 ng pk.GST, for the control, were used. A total of 700 ng of pk.GST or CYPA.GST together with 1,900 ng of pcDNA3.1 were used for the control. At 6 h posttransfection, 5 or 10 μM CsA or control DMSO was added to cells. At 48 h posttransfection, cells were lysed for 20 min on ice, followed by a 20-min centrifugation step at maximum speed in a benchtop centrifuge at 4°C. The supernatant of the cell lysate was added to GST beads together with viral lysates (obtained after 4 h of centrifugation under 20% sucrose at 4°C) and incubated according to the bead manufacturer's instructions (GE Healthcare, Solingen, Germany). Protein complexes were eluted from the beads and subjected to immunoblotting.

Immunoblotting. Cells were lysed for 20 min on ice using radioimmunoprecipitation assay (RIPA) buffer (25 mM Tris-HCl [pH 8.0], 137 mM NaCl, 1% NP-40, 1% glycerol, 0.5% sodium deoxycholate, 0.1% sodium dodecyl sulfate [SDS], 2 mM EDTA, and protease inhibitor cocktail set III [Calbiochem, Darmstadt, Germany]). The cell lysate was centrifuged at 14,800 rpm for 20 min at 4°C. Lysate protein denaturation was done for 5 min at 95°C in RotiLoad loading buffer (Roth, Karlsruhe, Germany), followed by Western blotting. CPSF6-358.HA was detected with mouse anti-HA (catalog number MMS-101P; Covance, Münster, Germany) (1:7,500 dilution). Tubulin was detected using an antitubulin antibody (clone DM1A, mouse monoclonal; Sigma-Aldrich) (1:20,000 dilution). CPSF6 was detected using an anti-CPSF6 antibody (rabbit polyclonal; Proteintech, Manchester, UK) (1:500 dilution). For TRIM5α detection, an anti-TRIM5 antibody was used (rabbit monoclonal, catalog number 143265; Cell Signaling Technology Europe BV, Frankfurt, Germany) (1:500 dilution). For NUP153 detection, an anti-NUP153 antibody was used (mouse monoclonal; Santa Cruz Biotechnology, Heidelberg, Germany) (1:500 dilution). An anti-NUP358 antibody (mouse monoclonal; Abcam, Cambridge, UK) (1:500 dilution) was used for NUP358 detection. For CYPA detection, an anti-CYPA antibody was used (mouse monoclonal; Santa Cruz Biotechnology) (1:500 dilution). CYPA.GST was detected using mouse anti-GST (kindly donated by Reza Ahmadian), and

TABLE 1 Homology modeling: templates used, sequence identities and similarities, and TopScore assessments

Model	Template	Sequence identity (%)	Sequence similarity (%)	TopScore[a]	TopScore Single[a]
PF74					
HIV1_PF74	4XFZ_A	92.2	92.2	0.17	0.17
	4QNB_A	92.2	92.2		
	4XRO_A	88.7	89.6		
	4U0E_A	89.6	89.6		
	6AXV_A	91.8	92.2		
SIVcpzPts_PF74	4XFZ_A	74.8	81.2	0.19	0.20
	4QNB_A	73.1	80.8		
	4XRO_A	71.0	78.6		
	4U0E_A	71.0	78.2		
	6AXV_A	74.6	81.6		
SIVcpzPtt_PF74	4XFZ_A	83.1	87.9	0.17	0.15
	4QNB_A	82.7	87.9		
	4XRO_A	80.5	85.7		
	4U0E_A	80.5	85.3		
	6AXV_A	82.7	87.9		
CPSF6					
HIV1_CPSF6	4WYM_A	90.9	90.9	0.19	0.17
	4U0A_A	88.3	88.3		
	6AY9_A	94.4	94.4		
	4B4N_A	58.9	58.9		
SIVcpzPts_CPSF6	4WYM_A	63.3	70.5	0.21	0.20
	4U0A_A	70.1	77.4		
	6AY9_A	75.2	81.6		
	4B4N_A	44.9	51.3		
SIVcpzPtt_CPSF6	4WYM_A	82.3	86.6	0.18	0.16
	4U0A_A	79.7	84.0		
	6AY9_A	84.9	89.6		
	4B4N_A	52.0	55.4		
Cyclophilin A					
HIV1_CYPA	5FJB_A	92.6	94.0	0.31	0.23
	1FGL_B	4.3	4.3		
	1M9D_C	60.2	60.6		
SIVcpzPts_CYPA	5FJB_A	74.0	81.6	0.33	0.28
	1FGL_B	2.1	2.6		
	1M9D_C	46.1	52.1		
SIVcpzPtt_CYPA	5FJB_A	84.0	89.6	0.31	0.23
	1FGL_B	3.5	3.9		
	1M9D_C	55.0	58.4		
Cyclophilin A	5FJB_C	99.4	99.4	0.09	0.17
	1FGL_A	100.0	100.0		
	1M9D_B	98.8	98.8		

[a]Lower TopScore or TopScore Single values indicate better structural quality. The values are bounded between 0 and 1.

p24/p27 monoclonal antibody (MAb) AG3.0 (1:250 dilution) was used to detect capsid p24. Anti-mouse antibody conjugated to horseradish peroxidase (catalog number NA931V; GE Healthcare) (1:10,000 dilution) and anti-rabbit antibody conjugated to horseradish peroxidase (catalog number NA9340V; GE Healthcare) (1:10,000 dilution) were used as secondary antibodies. Signals were visualized using ECL prime reagent (GE Healthcare).

Modeling of HIV-1, SIVcpzPts, and SIVcpzPtt CA protein-ligand structures. For each CA protein, three monomeric structures were built with TopModel (94) and validated with TopScore (73), one for each ligand. In addition, CYPA was modeled with TopModel (see Table 1 for the templates used). Hexameric structures were then constructed by alignment to the crystal structure of the HIV-1 CA protein (PDB accession number 4WYM) (31) using PyMOL 1.8. Finally, to generate three complex structures for each protein, ligands were inserted into the respective hexameric structures, using the position of PF74 from PDB accession number 4XFZ (95), the position of CPSF6 from PDB accession number 4WYM (31), and the position of CYPA from PDB accession number 1FGL (96) after superimposing the protein parts. For PF74, which was subsequently investigated in complex with the CA protein by molecular dynamics (MD) simulations and effective binding energy computations, superimposing was performed six times, to place PF74 in every binding pocket of the hexamer. For investigating CPSF6 and CYPA, for which only static complex structures were analyzed, this procedure was performed for one binding site only. Residues within 6 Å around the ligands were considered part of the binding pocket.

Molecular dynamics simulations of PF74 bound to HIV-1, SIVcpzPts, and SIVcpzPtt CA proteins. **(i) System setup.** For five replicas per hexameric CA protein-PF74 structure, MD simulations were performed with the Amber18 software package, resulting in a total of 15 MD simulations. Protonation states of protein residues and ligands were adjusted according to pH 7.4 using HTMD 1.12 (97). Atomic point charges of PF74 were generated according to the restrained electrostatic potential (RESP) procedure (98, 99), using antechamber (100) and GAUSSIAN16 (Rev. A.03) (101) at the HF/6-31G* level of theory. For the protein part, ff14SB force field parameters were used (102), and for the ligand, gaff2 force field parameters were used. Using tLEaP, the systems were solvated by an octahedral box of TIP3P water (103) such that the minimal distance between the box edge and any solute atom is 17 Å, and potassium ions were added to neutralize the charge of the systems (103).

(ii) Thermalization and production. Initially, the simulation systems (including the solute and solvent) were energy minimized using 10,000 steps of steepest-descent minimization, followed by 10,000 steps of conjugate gradient minimization, applying positional restraints on protein and ligand atoms with a force constant of 20 kcal mol^{-1} $Å^{-2}$. Second, the same minimization scheme was applied, now using positional restraints with a force constant of 20 kcal mol^{-1} $Å^{-2}$ on the protein atoms only. Finally, the systems were minimized using 20,000 steps of steepest-descent minimization, followed by 20,000 steps of conjugate gradient minimization, applying no restraints. Using NVT (constant number of particles, volume, and temperature) MD simulations, the systems were heated to 300 K using a constant heating rate over 210 ps and simulated for a further 70 ps at this temperature, with positional restraints with a force constant of 10.0 kcal mol^{-1} $Å^{-2}$ on protein and PF74 atoms. Subsequently, the density of the systems was adjusted using NPT (constant number of particles, pressure, and temperature) MD simulations and applying the Berendsen barostat for 1,300 ps, with positional restraints with a force constant of 2.0 kcal mol^{-1} $Å^{-2}$ on protein and PF74 atoms, followed by a final equilibration step of 1,720 ps in the NVT ensemble. For production, NVT MD simulations were performed for 200 ns, yielding an aggregate simulation time of $3 \times 5 \times 200$ ns $= 3$ μs, and coordinates were stored every 100 ps. For all simulations, the Langevin thermostat with a collision frequency of 2 ps^{-1} was used. Minimization and heating were performed on CPUs, and equilibration and production were performed on GPUs with PMEMD (104).

(iii) Calculation of effective binding energies. Effective binding energies were calculated using MMPBSA.py (74) from AmberTools19. For the calculation, the hexamers were split into six dimers containing one PF74 molecule each in the corresponding binding interface. Hence, 30 dimers per isoform were analyzed, corresponding to a total of 60,000 frames per isoform. We applied the 1-trajectory MM-PBSA approach, in which the snapshots of the complex, protein, and ligand are extracted from a single MD simulation of the complex (75). The polar part of the solvation free energy was computed with the linearized Poisson-Boltzmann equation using an internal dielectric constant of 4 and an external one of 80. The nonpolar part was computed using a surface tension of 0.0378 kcal mol^{-1} $Å^{-2}$ (105). To avoid any additional uncertainty in our calculations, we neglected contributions due to changes in the configurational entropy upon complex formation (106, 107).

The effective binding energies ($\Delta G_{effective}$) were averaged over five replicas, each containing six binding pockets ($\overline{\Delta G_{effective}}$). The distribution of $\Delta G_{effective}$ values is Gaussian, and no particular trends were observed over the simulation times. The SEM (standard error of the mean) over the 30 independent calculations for a system (SEM_{all}) was calculated by error propagation according to the following equation:

$$\mathrm{SEM_{all}} = \frac{1}{5 \times 6} \sqrt{\sum_{i=1}^{5} \sum_{j=1}^{6} \mathrm{SEM}_{i,j}^{\,2}}$$

In all cases, the statistical uncertainty (SEM_{all}) is <0.015 kcal mol^{-1} and, hence, below the chemical accuracy of 1 kcal mol^{-1}, which is the expected accuracy in an optimal case (76).

Protein sequence alignment. The alignment was generated with MAFFT (108) in Jalview (109). Jalview was also used to generate the Weblogos. The following randomly picked sequences were included in the analyses: HIV-1 M diverse subtypes (GenBank accession numbers A04321, AB023804, AB032740, AB049811, AB097865, AB098330, AB221005, AB221005, AB253421, AB485636, AB485638, AB485643, AB485646, AB485648, AB485656, AB485660, AB485662, AB703607, AB731663, AF110963, and AF190127, in addition to the sequence of the plasmid pMDLg/pRRE), SIVcpzPtt (GenBank accession numbers AF382828, AF103818.1, AF115393, AJ271369, AY169968, DQ373063, DQ373064, DQ373065, DQ373066, EF535993, FR686510, FR686511, GQ217539, JN091690, JN835461, JN835462, JX178450, and X52154), and SIVcpzPts (GenBank accession numbers AF447763, DQ374657, DQ374658, EF394356, EF394357, EF394358, JN091691, JN835460, JQ768416, JQ866001, and SIU42720).

Statistics. Statistical tests for significance (P value of <0.05) were performed with GraphPad Prism 5.

SUPPLEMENTAL MATERIAL

Supplemental material is available online only.

SUPPLEMENTAL FILE 1, PDF file, 0.6 MB.

ACKNOWLEDGMENTS

We thank Wioletta Hörschken and Björn Wefers for their excellent technical assistance. We thank Reza Ahmadian, Gilead Sciences, Thomas Gramberg, Beatrice H. Hahn, Frank Kirchhoff, Daniel Sauter, Heiner Schaal, Jonathan P. Stoye, Greg Towers, and

Stephen R. Yant for reagents and Felipe Diaz-Griffero and Neeltje Kootstra for discussions. The following reagents were obtained through the NIH AIDS Research and Reference Reagent Program, Division of AIDS, NIAID, NIH: psPAX2 (catalog number 11348) from Didier Trono and the SIVcpz TAN1.910 infectious molecular clone (catalog number 11496) from Jun Takehisa, Matthias H. Kraus, and Beatrice H. Hahn.

A.P.T. is supported by the German Academic Exchange Service (DAAD). Z.Z. was supported by the China Scholarship Council (CSC). C.M. is supported by the Heinz-Ansmann Foundation for AIDS Research. H.G. is grateful for computational support and infrastructure provided by the Zentrum für Informations und Medientechnologie (ZIM) at the Heinrich Heine University Düsseldorf and the computing time provided by the John von Neumann Institute for Computing (NIC) on the supercomputer JUWELS at the Jülich Supercomputing Centre (JSC) (user identifier HKF7).

REFERENCES

1. Bejarano DA, Peng K, Laketa V, Borner K, Jost KL, Lucic B, Glass B, Lusic M, Muller B, Krausslich H-G. 2019. HIV-1 nuclear import in macrophages is regulated by CPSF6-capsid interactions at the nuclear pore complex. Elife 8:e41800. https://doi.org/10.7554/eLife.41800.
2. Arhel NJ, Souquere-Besse S, Munier S, Souque P, Guadagnini S, Rutherford S, Prevost MC, Allen TD, Charneau P. 2007. HIV-1 DNA Flap formation promotes uncoating of the pre-integration complex at the nuclear pore. EMBO J 26:3025–3037. https://doi.org/10.1038/sj.emboj.7601740.
3. Francis AC, Melikyan GB. 2018. Single HIV-1 imaging reveals progression of infection through CA-dependent steps of docking at the nuclear pore, uncoating, and nuclear transport. Cell Host Microbe 23:536–548.e6. https://doi.org/10.1016/j.chom.2018.03.009.
4. Mamede JI, Cianci GC, Anderson MR, Hope TJ. 2017. Early cytoplasmic uncoating is associated with infectivity of HIV-1. Proc Natl Acad Sci U S A 114:E7169–E7178. https://doi.org/10.1073/pnas.1706245114.
5. Burdick RC, Li C, Munshi M, Rawson JMO, Nagashima K, Hu WS, Pathak VK. 2020. HIV-1 uncoats in the nucleus near sites of integration. Proc Natl Acad Sci U S A 117:5486–5493. https://doi.org/10.1073/pnas.1920631117.
6. Dharan A, Bachmann N, Talley S, Zwikelmaier V, Campbell EM. 2020. Nuclear pore blockade reveals that HIV-1 completes reverse transcription and uncoating in the nucleus. Nat Microbiol 5:1088–1095. https://doi.org/10.1038/s41564-020-0735-8.
7. Zurnic Bönisch I, Dirix L, Lemmens V, Borrenberghs D, De Wit F, Vernaillen F, Rocha S, Christ F, Hendrix J, Hofkens J, Debyser Z. 2020. Capsid-labelled HIV to investigate the role of capsid during nuclear import and integration. J Virol 94:e01024-19. https://doi.org/10.1128/JVI.01024-19.
8. Blair WS, Pickford C, Irving SL, Brown DG, Anderson M, Bazin R, Cao J, Ciaramella G, Isaacson J, Jackson L, Hunt R, Kjerrstrom A, Nieman JA, Patick AK, Perros M, Scott AD, Whitby K, Wu H, Butler SL. 2010. HIV capsid is a tractable target for small molecule therapeutic intervention. PLoS Pathog 6:e1001220. https://doi.org/10.1371/journal.ppat.1001220.
9. Lamorte L, Titolo S, Lemke CT, Goudreau N, Mercier JF, Wardrop E, Shah VB, von Schwedler UK, Langelier C, Banik SS, Aiken C, Sundquist WI, Mason SW. 2013. Discovery of novel small-molecule HIV-1 replication inhibitors that stabilize capsid complexes. Antimicrob Agents Chemother 57:4622–4631. https://doi.org/10.1128/AAC.00985-13.
10. Franke EK, Yuan HE, Luban J. 1994. Specific incorporation of cyclophilin A into HIV-1 virions. Nature 372:359–362. https://doi.org/10.1038/372359a0.
11. Thali M, Bukovsky A, Kondo E, Rosenwirth B, Walsh CT, Sodroski J, Gottlinger HG. 1994. Functional association of cyclophilin A with HIV-1 virions. Nature 372:363–365. https://doi.org/10.1038/372363a0.
12. Stremlau M, Owens CM, Perron MJ, Kiessling M, Autissier P, Sodroski J. 2004. The cytoplasmic body component TRIM5alpha restricts HIV-1 infection in Old World monkeys. Nature 427:848–853. https://doi.org/10.1038/nature02343.
13. Kane M, Yadav SS, Bitzegeio J, Kutluay SB, Zang T, Wilson SJ, Schoggins JW, Rice CM, Yamashita M, Hatziioannou T, Bieniasz PD. 2013. MX2 is an interferon-induced inhibitor of HIV-1 infection. Nature 502:563–566. https://doi.org/10.1038/nature12653.
14. Goujon C, Moncorge O, Bauby H, Doyle T, Ward CC, Schaller T, Hue S, Barclay WS, Schulz R, Malim MH. 2013. Human MX2 is an interferon-induced post-entry inhibitor of HIV-1 infection. Nature 502:559–562. https://doi.org/10.1038/nature12542.
15. Brass AL, Dykxhoorn DM, Benita Y, Yan N, Engelman A, Xavier RJ, Lieberman J, Elledge SJ. 2008. Identification of host proteins required for HIV infection through a functional genomic screen. Science 319:921–926. https://doi.org/10.1126/science.1152725.
16. König R, Zhou Y, Elleder D, Diamond TL, Bonamy GM, Irelan JT, Chiang CY, Tu BP, De Jesus PD, Lilley CE, Seidel S, Opaluch AM, Caldwell JS, Weitzman MD, Kuhen KL, Bandyopadhyay S, Ideker T, Orth AP, Miraglia LJ, Bushman FD, Young JA, Chanda SK. 2008. Global analysis of host-pathogen interactions that regulate early-stage HIV-1 replication. Cell 135:49–60. https://doi.org/10.1016/j.cell.2008.07.032.
17. Lee K, Ambrose Z, Martin TD, Oztop I, Mulky A, Julias JG, Vandegraaff N, Baumann JG, Wang R, Yuen W, Takemura T, Shelton K, Taniuchi I, Li Y, Sodroski J, Littman DR, Coffin JM, Hughes SH, Unutmaz D, Engelman A, KewalRamani VN. 2010. Flexible use of nuclear import pathways by HIV-1. Cell Host Microbe 7:221–233. https://doi.org/10.1016/j.chom.2010.02.007.
18. Schaller T, Ocwieja KE, Rasaiyaah J, Price AJ, Brady TL, Roth SL, Hue S, Fletcher AJ, Lee K, KewalRamani VN, Noursadeghi M, Jenner RG, James LC, Bushman FD, Towers GJ. 2011. HIV-1 capsid-cyclophilin interactions determine nuclear import pathway, integration targeting and replication efficiency. PLoS Pathog 7:e1002439. https://doi.org/10.1371/journal.ppat.1002439.
19. Matreyek KA, Yucel SS, Li X, Engelman A. 2013. Nucleoporin NUP153 phenylalanine-glycine motifs engage a common binding pocket within the HIV-1 capsid protein to mediate lentiviral infectivity. PLoS Pathog 9:e1003693. https://doi.org/10.1371/journal.ppat.1003693.
20. Mamede JI, Sitbon M, Battini JL, Courgnaud V. 2013. Heterogeneous susceptibility of circulating SIV isolate capsids to HIV-interacting factors. Retrovirology 10:77. https://doi.org/10.1186/1742-4690-10-77.
21. Jimenez-Guardeno JM, Apolonia L, Betancor G, Malim MH. 2019. Immunoproteasome activation enables human TRIM5alpha restriction of HIV-1. Nat Microbiol 4:933–940. https://doi.org/10.1038/s41564-019-0402-0.
22. Ohainle M, Kim K, Komurlu Keceli S, Felton A, Campbell E, Luban J, Emerman M. 2020. TRIM34 restricts HIV-1 and SIV capsids in a TRIM5alpha-dependent manner. PLoS Pathog 16:e1008507. https://doi.org/10.1371/journal.ppat.1008507.
23. Selyutina A, Persaud M, Simons LM, Bulnes-Ramos A, Buffone C, Martinez-Lopez A, Scoca V, Di Nunzio F, Hiatt J, Marson A, Krogan NJ, Hultquist JF, Diaz-Griffero F. 2020. Cyclophilin A prevents HIV-1 restriction in lymphocytes by blocking human TRIM5alpha binding to the viral core. Cell Rep 30:3766–3777.e6. https://doi.org/10.1016/j.celrep.2020.02.100.
24. De Iaco A, Luban J. 2011. Inhibition of HIV-1 infection by TNPO3 depletion is determined by capsid and detectable after viral cDNA enters the nucleus. Retrovirology 8:98. https://doi.org/10.1186/1742-4690-8-98.
25. Ning J, Zhong Z, Fischer DK, Harris G, Watkins SC, Ambrose Z, Zhang P. 2018. Truncated CPSF6 forms higher-order complexes that bind and disrupt HIV-1 capsid. J Virol 92:e00368-18. https://doi.org/10.1128/JVI.00368-18.

26. Merindol N, El-Far M, Sylla M, Masroori N, Dufour C, Li JX, Cherry P, Plourde MB, Tremblay C, Berthoux L. 2018. HIV-1 capsids from B27/B57+ elite controllers escape Mx2 but are targeted by TRIM5alpha, leading to the induction of an antiviral state. PLoS Pathog 14:e1007398. https://doi.org/10.1371/journal.ppat.1007398.
27. Maillard PV, Zoete V, Michielin O, Trono D. 2011. Homology-based identification of capsid determinants that protect HIV1 from human TRIM5alpha restriction. J Biol Chem 286:8128–8140. https://doi.org/10.1074/jbc.M110.187609.
28. Busnadiego I, Kane M, Rihn SJ, Preugschas HF, Hughes J, Blanco-Melo D, Strouvelle VP, Zang TM, Willett BJ, Boutell C, Bieniasz PD, Wilson SJ. 2014. Host and viral determinants of Mx2 antiretroviral activity. J Virol 88:7738–7752. https://doi.org/10.1128/JVI.00214-14.
29. Price AJ, Jacques DA, McEwan WA, Fletcher AJ, Essig S, Chin JW, Halambage UD, Aiken C, James LC. 2014. Host cofactors and pharmacologic ligands share an essential interface in HIV-1 capsid that is lost upon disassembly. PLoS Pathog 10:e1004459. https://doi.org/10.1371/journal.ppat.1004459.
30. Price AJ, Fletcher AJ, Schaller T, Elliott T, Lee K, KewalRamani VN, Chin JW, Towers GJ, James LC. 2012. CPSF6 defines a conserved capsid interface that modulates HIV-1 replication. PLoS Pathog 8:e1002896. https://doi.org/10.1371/journal.ppat.1002896.
31. Bhattacharya A, Alam SL, Fricke T, Zadrozny K, Sedzicki J, Taylor AB, Demeler B, Pornillos O, Ganser-Pornillos BK, Diaz-Griffero F, Ivanov DN, Yeager M. 2014. Structural basis of HIV-1 capsid recognition by PF74 and CPSF6. Proc Natl Acad Sci U S A 111:18625–18630. https://doi.org/10.1073/pnas.1419945112.
32. Shi J, Zhou J, Shah VB, Aiken C, Whitby K. 2011. Small-molecule inhibition of human immunodeficiency virus type 1 infection by virus capsid destabilization. J Virol 85:542–549. https://doi.org/10.1128/JVI.01406-10.
33. Saito A, Ferhadian D, Sowd GA, Serrao E, Shi J, Halambage UD, Teng S, Soto J, Siddiqui MA, Engelman AN, Aiken C, Yamashita M. 2016. Roles of capsid-interacting host factors in multimodal inhibition of HIV-1 by PF74. J Virol 90:5808–5823. https://doi.org/10.1128/JVI.03116-15.
34. Hulme AE, Kelley Z, Foley D, Hope TJ. 2015. Complementary assays reveal a low level of CA associated with viral complexes in the nuclei of HIV-1-infected cells. J Virol 89:5350–5361. https://doi.org/10.1128/JVI.00476-15.
35. Balasubramaniam M, Zhou J, Addai A, Martinez P, Pandhare J, Aiken C, Dash C. 2019. PF74 inhibits HIV-1 integration by altering the composition of the preintegration complex. J Virol 93:e01741-18. https://doi.org/10.1128/JVI.01741-18.
36. Carnes SK, Sheehan JH, Aiken C. 2018. Inhibitors of the HIV-1 capsid, a target of opportunity. Curr Opin HIV AIDS 13:359–365. https://doi.org/10.1097/COH.0000000000000472.
37. Singh K, Gallazzi F, Hill KJ, Burke DH, Lange MJ, Quinn TP, Neogi U, Sonnerborg A. 2019. GS-CA compounds: first-in-class HIV-1 capsid inhibitors covering multiple grounds. Front Microbiol 10:1227. https://doi.org/10.3389/fmicb.2019.01227.
38. Yant SR, Mulato A, Hansen D, Tse WC, Niedziela-Majka A, Zhang JR, Stepan GJ, Jin D, Wong MH, Perreira JM, Singer E, Papalia GA, Hu EY, Zheng J, Lu B, Schroeder SD, Chou K, Ahmadyar S, Liclican A, Yu H, Novikov N, Paoli E, Gonik D, Ram RR, Hung M, McDougall WM, Brass AL, Sundquist WI, Cihlar T, Link JO. 2019. A highly potent long-acting small-molecule HIV-1 capsid inhibitor with efficacy in a humanized mouse model. Nat Med 25:1377–1384. https://doi.org/10.1038/s41591-019-0560-x.
39. Twizerimana AP, Scheck R, Häussinger D, Münk C. 2018. Post-entry restriction factors of SIVcpz. Future Virol 13:727–745. https://doi.org/10.2217/fvl-2018-0093.
40. Sharp PM, Hahn BH. 2010. The evolution of HIV-1 and the origin of AIDS. Philos Trans R Soc Lond B Biol Sci 365:2487–2494. https://doi.org/10.1098/rstb.2010.0031.
41. Gao F, Bailes E, Robertson DL, Chen Y, Rodenburg CM, Michael SF, Cummins LB, Arthur LO, Peeters M, Shaw GM, Sharp PM, Hahn BH. 1999. Origin of HIV-1 in the chimpanzee Pan troglodytes troglodytes. Nature 397:436–441. https://doi.org/10.1038/17130.
42. Zhang Z, Gu Q, de Manuel Montero M, Bravo IG, Marques-Bonet T, Häussinger D, Münk C. 2017. Stably expressed APOBEC3H forms a barrier for cross-species transmission of simian immunodeficiency virus of chimpanzee to humans. PLoS Pathog 13:e1006746. https://doi.org/10.1371/journal.ppat.1006746.
43. Sauter D, Schindler M, Specht A, Landford WN, Munch J, Kim KA, Votteler J, Schubert U, Bibollet-Ruche F, Keele BF, Takehisa J, Ogando Y, Ochsenbauer C, Kappes JC, Ayouba A, Peeters M, Learn GH, Shaw G, Sharp PM, Bieniasz P, Hahn BH, Hatziioannou T, Kirchhoff F. 2009. Tetherin-driven adaptation of Vpu and Nef function and the evolution of pandemic and nonpandemic HIV-1 strains. Cell Host Microbe 6:409–421. https://doi.org/10.1016/j.chom.2009.10.004.
44. Kratovac Z, Virgen CA, Bibollet-Ruche F, Hahn BH, Bieniasz PD, Hatziioannou T. 2008. Primate lentivirus capsid sensitivity to TRIM5 proteins. J Virol 82:6772–6777. https://doi.org/10.1128/JVI.00410-08.
45. Meier K, Jaguva Vasudevan AA, Zhang Z, Bahr A, Kochs G, Häussinger D, Münk C. 2018. Equine MX2 is a restriction factor of equine infectious anemia virus (EIAV). Virology 523:52–63. https://doi.org/10.1016/j.virol.2018.07.024.
46. McEwan WA, Schaller T, Ylinen LM, Hosie MJ, Towers GJ, Willett BJ. 2009. Truncation of TRIM5 in the Feliformia explains the absence of retroviral restriction in cells of the domestic cat. J Virol 83:8270–8275. https://doi.org/10.1128/JVI.00670-09.
47. Bieniasz PD. 2004. Intrinsic immunity: a front-line defense against viral attack. Nat Immunol 5:1109–1115. https://doi.org/10.1038/ni1125.
48. Münk C, Brandt SM, Lucero G, Landau NR. 2002. A dominant block to HIV-1 replication at reverse transcription in simian cells. Proc Natl Acad Sci U S A 99:13843–13848. https://doi.org/10.1073/pnas.212400099.
49. Cowan S, Hatziioannou T, Cunningham T, Muesing MA, Gottlinger HG, Bieniasz PD. 2002. Cellular inhibitors with Fv1-like activity restrict human and simian immunodeficiency virus tropism. Proc Natl Acad Sci U S A 99:11914–11919. https://doi.org/10.1073/pnas.162299499.
50. Besnier C, Takeuchi Y, Towers G. 2002. Restriction of lentivirus in monkeys. Proc Natl Acad Sci U S A 99:11920–11925. https://doi.org/10.1073/pnas.172384599.
51. Lu M, Hou G, Zhang H, Suiter CL, Ahn J, Byeon IJ, Perilla JR, Langmead CJ, Hung I, Gor'kov PL, Gan Z, Brey W, Aiken C, Zhang P, Schulten K, Gronenborn AM, Polenova T. 2015. Dynamic allostery governs cyclophilin A-HIV capsid interplay. Proc Natl Acad Sci U S A 112:14617–14622. https://doi.org/10.1073/pnas.1516920112.
52. Liu Z, Pan Q, Ding S, Qian J, Xu F, Zhou J, Cen S, Guo F, Liang C. 2013. The interferon-inducible MxB protein inhibits HIV-1 infection. Cell Host Microbe 14:398–410. https://doi.org/10.1016/j.chom.2013.08.015.
53. Rasaiyaah J, Tan CP, Fletcher AJ, Price AJ, Blondeau C, Hilditch L, Jacques DA, Selwood DL, James LC, Noursadeghi M, Towers GJ. 2013. HIV-1 evades innate immune recognition through specific cofactor recruitment. Nature 503:402–405. https://doi.org/10.1038/nature12769.
54. Ambrose Z, Lee K, Ndjomou J, Xu H, Oztop I, Matous J, Takemura T, Unutmaz D, Engelman A, Hughes SH, KewalRamani VN. 2012. Human immunodeficiency virus type 1 capsid mutation N74D alters cyclophilin A dependence and impairs macrophage infection. J Virol 86:4708–4714. https://doi.org/10.1128/JVI.05887-11.
55. Qi M, Yang R, Aiken C. 2008. Cyclophilin A-dependent restriction of human immunodeficiency virus type 1 capsid mutants for infection of nondividing cells. J Virol 82:12001–12008. https://doi.org/10.1128/JVI.01518-08.
56. Sokolskaja E, Sayah DM, Luban J. 2004. Target cell cyclophilin A modulates human immunodeficiency virus type 1 infectivity. J Virol 78:12800–12808. https://doi.org/10.1128/JVI.78.23.12800-12808.2004.
57. Burse M, Shi J, Aiken C. 2017. Cyclophilin A potentiates TRIM5alpha inhibition of HIV-1 nuclear import without promoting TRIM5alpha binding to the viral capsid. PLoS One 12:e0182298. https://doi.org/10.1371/journal.pone.0182298.
58. Sokolskaja E, Luban J. 2006. Cyclophilin, TRIM5, and innate immunity to HIV-1. Curr Opin Microbiol 9:404–408. https://doi.org/10.1016/j.mib.2006.06.011.
59. Kootstra NA, Münk C, Tonnu N, Landau NR, Verma IM. 2003. Abrogation of postentry restriction of HIV-1-based lentiviral vector transduction in simian cells. Proc Natl Acad Sci U S A 100:1298–1303. https://doi.org/10.1073/pnas.0337541100.
60. Shah VB, Shi J, Hout DR, Oztop I, Krishnan L, Ahn J, Shotwell MS, Engelman A, Aiken C. 2013. The host proteins transportin SR2/TNPO3 and cyclophilin A exert opposing effects on HIV-1 uncoating. J Virol 87:422–432. https://doi.org/10.1128/JVI.07177-11.
61. De Iaco A, Luban J. 2014. Cyclophilin A promotes HIV-1 reverse transcription but its effect on transduction correlates best with its effect on nuclear entry of viral cDNA. Retrovirology 11:11. https://doi.org/10.1186/1742-4690-11-11.
62. Luban J, Bossolt KL, Franke EK, Kalpana GV, Goff SP. 1993. Human

immunodeficiency virus type 1 Gag protein binds to cyclophilins A and B. Cell 73:1067–1078. https://doi.org/10.1016/0092-8674(93)90637-6.
63. Gamble TR, Vajdos FF, Yoo S, Worthylake DK, Houseweart M, Sundquist WI, Hill CP. 1996. Crystal structure of human cyclophilin A bound to the amino-terminal domain of HIV-1 capsid. Cell 87:1285–1294. https://doi.org/10.1016/s0092-8674(00)81823-1.
64. Franke EK, Luban J. 1996. Inhibition of HIV-1 replication by cyclosporine A or related compounds correlates with the ability to disrupt the Gag-cyclophilin A interaction. Virology 222:279–282. https://doi.org/10.1006/viro.1996.0421.
65. Yin L, Braaten D, Luban J. 1998. Human immunodeficiency virus type 1 replication is modulated by host cyclophilin A expression levels. J Virol 72:6430–6436. https://doi.org/10.1128/JVI.72.8.6430-6436.1998.
66. Braaten D, Franke EK, Luban J. 1996. Cyclophilin A is required for an early step in the life cycle of human immunodeficiency virus type 1 before the initiation of reverse transcription. J Virol 70:3551–3560. https://doi.org/10.1128/JVI.70.6.3551-3560.1996.
67. Braaten D, Franke EK, Luban J. 1996. Cyclophilin A is required for the replication of group M human immunodeficiency virus type 1 (HIV-1) and simian immunodeficiency virus SIV(CPZ)GAB but not group O HIV-1 or other primate immunodeficiency viruses. J Virol 70:4220–4227. https://doi.org/10.1128/JVI.70.7.4220-4227.1996.
68. Hatziioannou T, Perez-Caballero D, Cowan S, Bieniasz PD. 2005. Cyclophilin interactions with incoming human immunodeficiency virus type 1 capsids with opposing effects on infectivity in human cells. J Virol 79:176–183. https://doi.org/10.1128/JVI.79.1.176-183.2005.
69. Mlynar E, Bevec D, Billich A, Rosenwirth B, Steinkasserer A. 1997. The non-immunosuppressive cyclosporin A analogue SDZ NIM 811 inhibits cyclophilin A incorporation into virions and virus replication in human immunodeficiency virus type 1-infected primary and growth-arrested T cells. J Gen Virol 78(Part 4):825–835. https://doi.org/10.1099/0022-1317-78-4-825.
70. Saini M, Potash MJ. 2006. Novel activities of cyclophilin A and cyclosporin A during HIV-1 infection of primary lymphocytes and macrophages. J Immunol 177:443–449. https://doi.org/10.4049/jimmunol.177.1.443.
71. Towers GJ, Hatziioannou T, Cowan S, Goff SP, Luban J, Bieniasz PD. 2003. Cyclophilin A modulates the sensitivity of HIV-1 to host restriction factors. Nat Med 9:1138–1143. https://doi.org/10.1038/nm910.
72. Saito A, Henning MS, Serrao E, Dubose BN, Teng S, Huang J, Li X, Saito N, Roy SP, Siddiqui MA, Ahn J, Tsuji M, Hatziioannou T, Engelman AN, Yamashita M. 2016. Capsid-CPSF6 interaction is dispensable for HIV-1 replication in primary cells but is selected during virus passage in vivo. J Virol 90:6918–6935. https://doi.org/10.1128/JVI.00019-16.
73. Mulnaes D, Gohlke H. 2018. TopScore: using deep neural networks and large diverse data sets for accurate protein model quality assessment. J Chem Theory Comput 14:6117–6126. https://doi.org/10.1021/acs.jctc.8b00690.
74. Miller BR, McGee TD, Swails JM, Homeyer N, Gohlke H, Roitberg AE. 2012. MMPBSA.py: an efficient program for end-state free energy calculations. J Chem Theory Comput 8:3314–3321. https://doi.org/10.1021/ct300418h.
75. Homeyer N, Gohlke H. 2012. Free energy calculations by the molecular mechanics Poisson-Boltzmann surface area method. Mol Inform 31:114–122. https://doi.org/10.1002/minf.201100135.
76. Michel J, Essex JW. 2010. Prediction of protein-ligand binding affinity by free energy simulations: assumptions, pitfalls and expectations. J Comput Aided Mol Des 24:639–658. https://doi.org/10.1007/s10822-010-9363-3.
77. Rankovic S, Ramalho R, Aiken C, Rousso I. 2018. PF74 reinforces the HIV-1 capsid to impair reverse transcription-induced uncoating. J Virol 92:e00845-18. https://doi.org/10.1128/JVI.00845-18.
78. Fricke T, Buffone C, Opp S, Valle-Casuso J, Diaz-Griffero F. 2014. Bl-2 destabilizes HIV-1 cores during infection and prevents binding of CPSF6 to the HIV-1 capsid. Retrovirology 11:120. https://doi.org/10.1186/s12977-014-0120-x.
79. Buffone C, Martinez-Lopez A, Fricke T, Opp S, Severgnini M, Cifola I, Petiti L, Frabetti S, Skorupka K, Zadrozny KK, Ganser-Pornillos BK, Pornillos O, Di Nunzio F, Diaz-Griffero F. 2018. Nup153 unlocks the nuclear pore complex for HIV-1 nuclear translocation in nondividing cells. J Virol 92:e00648-18. https://doi.org/10.1128/JVI.00648-18.
80. Zhou J, Price AJ, Halambage UD, James LC, Aiken C. 2015. HIV-1 resistance to the capsid-targeting inhibitor PF74 results in altered dependence on host factors required for virus nuclear entry. J Virol 89:9068–9079. https://doi.org/10.1128/JVI.00340-15.
81. Lahaye X, Satoh T, Gentili M, Cerboni S, Silvin A, Conrad C, Ahmed-Belkacem A, Rodriguez EC, Guichou JF, Bosquet N, Piel M, Le Grand R, King MC, Pawlotsky JM, Manel N. 2016. Nuclear envelope protein SUN2 promotes cyclophilin-A-dependent steps of HIV replication. Cell Rep 15:879–892. https://doi.org/10.1016/j.celrep.2016.03.074.
82. De laco A, Santoni F, Vannier A, Guipponi M, Antonarakis S, Luban J. 2013. TNPO3 protects HIV-1 replication from CPSF6-mediated capsid stabilization in the host cell cytoplasm. Retrovirology 10:20. https://doi.org/10.1186/1742-4690-10-20.
83. Hori T, Takeuchi H, Saito H, Sakuma R, Inagaki Y, Yamaoka S. 2013. A carboxy-terminally truncated human CPSF6 lacking residues encoded by exon 6 inhibits HIV-1 cDNA synthesis and promotes capsid disassembly. J Virol 87:7726–7736. https://doi.org/10.1128/JVI.00124-13.
84. Lee K, Mulky A, Yuen W, Martin TD, Meyerson NR, Choi L, Yu H, Sawyer SL, KewalRamani VN. 2012. HIV-1 capsid-targeting domain of cleavage and polyadenylation specificity factor 6. J Virol 86:3851–3860. https://doi.org/10.1128/JVI.06607-11.
85. Kane M, Rebensburg SV, Takata MA, Zang TM, Yamashita M, Kvaratskhelia M, Bieniasz PD. 2018. Nuclear pore heterogeneity influences HIV-1 infection and the antiviral activity of MX2. Elife 7:e35738. https://doi.org/10.7554/eLife.35738.
86. Bock M, Bishop KN, Towers G, Stoye JP. 2000. Use of a transient assay for studying the genetic determinants of Fv1 restriction. J Virol 74:7422–7430. https://doi.org/10.1128/jvi.74.16.7422-7430.2000.
87. Takehisa J, Kraus MH, Decker JM, Li Y, Keele BF, Bibollet-Ruche F, Zammit KP, Weng Z, Santiago ML, Kamenya S, Wilson ML, Pusey AE, Bailes E, Sharp PM, Shaw GM, Hahn BH. 2007. Generation of infectious molecular clones of simian immunodeficiency virus from fecal consensus sequences of wild chimpanzees. J Virol 81:7463–7475. https://doi.org/10.1128/JVI.00551-07.
88. Bibollet-Ruche F, Heigele A, Keele BF, Easlick JL, Decker JM, Takehisa J, Learn G, Sharp PM, Hahn BH, Kirchhoff F. 2012. Efficient SIVcpz replication in human lymphoid tissue requires viral matrix protein adaptation. J Clin Invest 122:1644–1652. https://doi.org/10.1172/JCI61429.
89. Bähr A, Singer A, Hain A, Vasudevan AA, Schilling M, Reh J, Riess M, Panitz S, Serrano V, Schweizer M, Konig R, Chanda S, Häussinger D, Kochs G, Lindemann D, Münk C. 2016. Interferon but not MxB inhibits foamy retroviruses. Virology 488:51–60. https://doi.org/10.1016/j.virol.2015.10.034.
90. Dull T, Zufferey R, Kelly M, Mandel RJ, Nguyen M, Trono D, Naldini L. 1998. A third-generation lentivirus vector with a conditional packaging system. J Virol 72:8463–8471. https://doi.org/10.1128/JVI.72.11.8463-8471.1998.
91. Osei Kuffour E, Schott K, Jaguva Vasudevan AA, Holler J, Schulz WA, Lang PA, Lang KS, Kim B, Häussinger D, König R, Münk C. 2018. USP18 (UBP43) abrogates p21-mediated inhibition of HIV-1. J Virol 92:e00592-18. https://doi.org/10.1128/JVI.00592-18.
92. Shalem O, Sanjana NE, Hartenian E, Shi X, Scott DA, Mikkelson T, Heckl D, Ebert BL, Root DE, Doench JG, Zhang F. 2014. Genome-scale CRISPR-Cas9 knockout screening in human cells. Science 343:84–87. https://doi.org/10.1126/science.1247005.
93. Sanjana NE, Shalem O, Zhang F. 2014. Improved vectors and genome-wide libraries for CRISPR screening. Nat Methods 11:783–784. https://doi.org/10.1038/nmeth.3047.
94. Mulnaes D, Porta N, Clemens R, Apanasenko I, Reiners J, Gremer L, Neudecker P, Smits SHJ, Gohlke H. 2020. TopModel: template-based protein structure prediction at low sequence identity using top-down consensus and deep neural networks. J Chem Theory Comput 16:1953–1967. https://doi.org/10.1021/acs.jctc.9b00825.
95. Gres AT, Kirby KA, KewalRamani VN, Tanner JJ, Pornillos O, Sarafianos SG. 2015. Structural virology. X-ray crystal structures of native HIV-1 capsid protein reveal conformational variability. Science 349:99–103. https://doi.org/10.1126/science.aaa5936.
96. Zhao Y, Chen Y, Schutkowski M, Fischer G, Ke H. 1997. Cyclophilin A complexed with a fragment of HIV-1 Gag protein: insights into HIV-1 infectious activity. Structure 5:139–146. https://doi.org/10.1016/s0969-2126(97)00172-x.
97. Doerr S, Harvey MJ, Noé F, De Fabritiis G. 2016. HTMD: high-throughput molecular dynamics for molecular discovery. J Chem Theory Comput 12:1845–1852. https://doi.org/10.1021/acs.jctc.6b00049.
98. Bayly CI, Cieplak P, Cornell W, Kollman PA. 1993. A well-behaved electrostatic potential based method using charge restraints for deriv-

ing atomic charges: the RESP model. J Phys Chem 97:10269–10280. https://doi.org/10.1021/j100142a004.
99. Wang J, Cieplak P, Kollman PA. 2000. How well does a restrained electrostatic potential (RESP) model perform in calculating conformational energies of organic and biological molecules? J Comput Chem 21:1049–1074. https://doi.org/10.1002/1096-987X(200009)21:12<1049::AID-JCC3>3.0.CO;2-F.
100. Wang J, Wang W, Kollman PA, Case DA. 2006. Automatic atom type and bond type perception in molecular mechanical calculations. J Mol Graph Model 25:247–260. https://doi.org/10.1016/j.jmgm.2005.12.005.
101. Frisch MJ, Trucks GW, Schlegel HB, Scuseria GE, Robb MA, Cheeseman JR, Scalmani G, Barone V, Petersson GA, Nakatsuji H, Li X, Caricato M, Marenich AV, Bloino J, Janesko BG, Gomperts R, Mennucci B, Hratchian HP, Ortiz JV, Izmaylov AF, Sonnenberg JL, Williams-Young D, Ding F, Lipparini F, Egidi F, Goings J, Peng B, Petrone A, Henderson T, Ranasinghe D, Zakrzewski VG, Gao J, Rega N, Zheng G, Liang W, Hada M, Ehara M, Toyota K, Fukuda R, Hasegawa J, Ishida M, Nakajima T, Honda Y, Kitao O, Nakai H, Vreven T, Throssell K, Montgomery JA, Jr, Peralta JE, Ogliaro F, et al. 2016. Gaussian 16 Rev. C.01. Gaussian Inc, Wallingford, CT.
102. Maier JA, Martinez C, Kasavajhala K, Wickstrom L, Hauser KE, Simmerling C. 2015. ff14SB: improving the accuracy of protein side chain and backbone parameters from ff99SB. J Chem Theory Comput 11:3696–3713. https://doi.org/10.1021/acs.jctc.5b00255.
103. Jorgensen WL, Chandrasekhar J, Madura JD, Impey RW, Klein ML. 1983. Comparison of simple potential functions for simulating liquid water. J Chem Phys 79:926–935. https://doi.org/10.1063/1.445869.
104. Salomon-Ferrer R, Götz AW, Poole D, Le Grand S, Walker RC. 2013. Routine microsecond molecular dynamics simulations with AMBER on GPUs. 2. Explicit solvent particle mesh Ewald. J Chem Theory Comput 9:3878–3888. https://doi.org/10.1021/ct400314y.
105. Tan C, Tan Y-H, Luo R. 2007. Implicit nonpolar solvent models. J Phys Chem B 111:12263–12274. https://doi.org/10.1021/jp073399n.
106. Gohlke H, Case DA. 2004. Converging free energy estimates: MM-PB(GB)SA studies on the protein-protein complex Ras-Raf. J Comput Chem 25:238–250. https://doi.org/10.1002/jcc.10379.
107. Hou T, Wang J, Li Y, Wang W. 2011. Assessing the performance of the MM/PBSA and MM/GBSA methods. 1. The accuracy of binding free energy calculations based on molecular dynamics simulations. J Chem Inf Model 51:69–82. https://doi.org/10.1021/ci100275a.
108. Katoh K, Standley DM. 2013. MAFFT multiple sequence alignment software version 7: improvements in performance and usability. Mol Biol Evol 30:772–780. https://doi.org/10.1093/molbev/mst010.
109. Waterhouse AM, Procter JB, Martin DM, Clamp M, Barton GJ. 2009. Jalview version 2—a multiple sequence alignment editor and analysis workbench. Bioinformatics 25:1189–1191. https://doi.org/10.1093/bioinformatics/btp033.